

Calculated phase equilibria in K_2O -FeO-MgO- Al_2O_3 -SiO₂-H₂O for sapphirine-quartz-bearing mineral assemblages

D. E. KELSEY,¹ R. W. WHITE,¹ T. J. B. HOLLAND² AND R. POWELL¹

¹School of Earth Sciences, University of Melbourne, Victoria 3010, Australia (snaredaveyk@yahoo.com.au)

²Department of Earth Sciences, University of Cambridge, Cambridge, CB2 3EQ, UK

ABSTRACT

Sapphirine, coexisting with quartz, is an indicator mineral for ultrahigh-temperature metamorphism in aluminous rock compositions. Here a new activity-composition model for sapphirine is combined with the internally consistent thermodynamic dataset used by THERMOCALC, for calculations primarily in K_2O -FeO-MgO- Al_2O_3 -SiO₂-H₂O (KFMASH). A discrepancy between published experimentally derived FMAS grids and our calculations is understood with reference to H₂O. Published FMAS grids effectively represent constant a_{H_2O} sections, thereby limiting their detailed use for the interpretation of mineral reaction textures in compositions with differing H₂O. For the calculated KFMASH univariant reaction grid, sapphirine + quartz assemblages occur at P - T in excess of 6–7 kbar and 1005 °C. Sapphirine compositions and composition ranges are consistent with natural examples. However, as many univariant equilibria are typically not ‘seen’ by a specific bulk composition, the univariant reaction grid may reveal little about the detailed topology of multi-variant equilibria, and therefore is of limited use for interpreting the P - T evolution of mineral assemblages and reaction sequences. Calculated pseudosections, which quantify bulk composition and multi-variant equilibria, predict experimentally determined KFMASH mineral assemblages with consistent topology, and also indicate that sapphirine stabilizes at increasingly higher pressure and temperature as X_{Mg} increases. Although coexisting sapphirine and quartz can occur in relatively iron-rich rocks if the bulk chemistry is sufficiently aluminous, the P - T window of stability shrinks with decreasing X_{Mg} . An array of mineral assemblages and mineral reaction sequences from natural sapphirine + quartz and other rocks from Enderby Land, Antarctica, are reproducible with calculated pseudosections. That consistent phase diagram calculations involving sapphirine can be performed allows for a more thorough assessment of the metamorphic evolution of high-temperature granulite facies terranes than was previously possible. The establishment of a a - x model for sapphirine provides the basis for expansion to larger, more geologically realistic chemical systems (e.g. involving Fe³⁺).

Key words: a_{H_2O} ; granulite; pseudosection; THERMOCALC; ultrahigh-temperature metamorphism.

Mineral abbreviations: bi, biotite; cd, cordierite; g, garnet; ksp, K-feldspar; ky, kyanite; liq, silicate melt; mu, muscovite; opx, orthopyroxene; osm, osumilite; q, quartz; sa, sapphirine; sill, sillimanite; sp, spinel.

INTRODUCTION

Sapphirine is an indicator mineral for high-temperature granulite facies metamorphic conditions in aluminous and/or metapelitic rock compositions. Some of the highest temperature conditions of crustal metamorphism are indicated by the association of sapphirine with quartz (see reviews in Harley, 1989, 1998a,b). However, the quantitative interpretation of the metamorphic evolution of sapphirine-bearing mineral assemblages has long presented a problem, due in part to a relatively poor understanding of the thermodynamic properties of sapphirine. Consequently, most studies of sapphirine-bearing granulite facies rocks present dominantly qualitative interpretations of the metamorphic P - T evolution.

Qualitative, experimentally constrained and semi-quantitative pressure-temperature (P - T) projections depicting univariant reactions have been proposed

and applied to interpret sapphirine-bearing mineral assemblages in various model chemical systems, including MAS (MgO- Al_2O_3 -SiO₂; Harley & Motoyoshi, 2000; Hollis & Harley, 2003), FMAS (+ FeO; Hensen, 1971, 1986; Harley, 1989, 1998a), FMASH (+ H₂O; Bertrand *et al.*, 1991), FMASO (+ Fe₂O₃; Hensen, 1986), FMASHO (Bertrand *et al.*, 1991), FMASTO (+ TiO₂; Powell & Sandiford, 1988), KMASH (+ K₂O; Grew, 1982), KFMAS (Ellis *et al.*, 1980; Grew, 1982), KFMASH (Hensen & Harley, 1990; Audibert *et al.*, 1995; Carrington & Harley, 1995a,b; McDade & Harley, 2001; Ouzegane *et al.*, 2003), KFMASO (Sandiford *et al.*, 1987) and KFMASHO (Dasgupta *et al.*, 1995; Das *et al.*, 2001, 2003). Unfortunately, there remains uncertainty regarding the location of such grids in P - T space, thereby influencing P - T estimates obtained for mineral assemblages depicted by such grids. However, natural mineral assemblages will typically evolve via

multi-variant, rather than univariant, equilibria (e.g. Stüwe & Powell, 1995; White *et al.*, 2002; Kelsey *et al.*, 2003a,b). Thus, calculated mineral equilibria, in the form of P - T pseudosections, can provide a more reliable means of interpreting the evolution of a mineral assemblage as bulk composition (X) and multi-variant (variance, $\nu \geq 2$) mineral equilibria are accounted for (e.g. Powell *et al.*, 1998; White *et al.*, 2002).

In this contribution a new activity-composition (a - x) model for sapphirine is presented for use in THERMOCALC (Powell & Holland, 1988; Holland & Powell, 1998, with subsequent updates). Using this new model, phase diagrams are calculated to serve two main purposes. First, to provide a quantitative explanation for the uncertainty associated with the P - T location of commonly used grids in the literature; and secondly, to investigate the P - T - X stability and evolution of sapphirine-quartz-bearing mineral assemblages in KFMASH, citing rocks from Enderby Land, Antarctica, as an example. KFMASH is the smallest chemical system in which the relevant mineral equilibria can be established, forming the 'backbone' for mineral equilibria in larger systems (White *et al.*, 2001, 2002).

The sapphirine model presented here differs from the sapphirine a - x model in Holland & Powell (1998), which was used in a modified form by Ouzegane *et al.* (2003) such that their partial grid calculations were consistent with experimental data of Hensen & Green (1973). Examples using the new sapphirine a - x model in this study will be restricted to quartz-bearing assemblages. Our new sapphirine model is also applicable to silica-undersaturated assemblages, although the interpretation of such assemblages requires the underlying quartz-absent P - T grid, which is to be the subject of a later contribution. In comparing the model results with existing data, the discussion will largely be restricted to comparisons with recent KFMASH (minimal Fe^{3+}) experiments, particularly those of Audibert *et al.* (1995).

AN A-X MODEL FOR SAPPHIRINE

The preliminary model and thermodynamic data for sapphirine in Holland & Powell (1998) was only consistent with silica-undersaturated experiments. As that model was inconsistent with quartz-bearing experiments in MAS, FMAS, etc., predicting invariant point temperatures > 1100 °C and incorrect topology, it is replaced by the following a - x model in which the silica-saturated and -undersaturated experimental data have been reconciled. The new model is applicable for calculations in the system KFMASH and its subsystems. The model does not incorporate Fe^{3+} , which is widely recognized as affecting the topology of phase relationships in sapphirine-bearing granulites, owing mainly to the enhanced stability of spinel (e.g. Annersten & Seifert, 1981; Hensen, 1986; Powell & Sandiford, 1988; Das *et al.*, 2001, 2003), but also that of sapphirine (e.g. Steffen *et al.*, 1984; Sandiford *et al.*, 1987; Powell & Sandiford, 1988).

The sapphirine model is characterized by two dominant cation substitutions, namely Fe-Mg and Tschermaks (AlAl-Si[Fe,Mg]) (e.g. Moore, 1969; Higgins *et al.*, 1979; Christy *et al.*, 1992). Of the eight octahedral (M1-8) and six tetrahedral (T1-6) sites only the M3 and T3 sites in sapphirine display significant multi-element (Mg, Al, Si)

Table 1. Site-distribution in the three sapphirine end-members (EM).

EM	M3	M46	T3	x	y
spr4	Mg	Mg ₃	Si	0	0
fspr	Fe	Fe ₃	Si	1	0
spr5	Al	Mg ₃	Al	0	1

substitution (e.g. Christy *et al.*, 1992). In addition, Fe-Mg mixing is modelled on three octahedral sites, M4-6. Thus, as a first approximation, element substitution is modelled to occur only on the M3, T3 and M46 sites. In the absence of information to the contrary, Fe-Mg equipartitioning is assumed. The end-members 2:2:1 spr4 (Mg₄Al₈Si₂O₂₀), 2:2:1 fspr (Fe₄Al₈Si₂O₂₀) and 3:5:1 spr5 (Mg₃Al₁₀Si₂O₂₀) are chosen to represent the solid-solution in sapphirine (Table 1), as these are considered to span the range of naturally occurring (K)FMAS(H) sapphirine compositions in quartz-bearing and quartz-absent rocks.

Two variables, x and y , are required to describe the composition of sapphirine. The composition variables are defined as:

$$x_{\text{sa}} = \frac{(x_{\text{Fe}}^{\text{M3}} + 3x_{\text{Fe}}^{\text{M46}})}{(x_{\text{Fe}}^{\text{M3}} + 3x_{\text{Fe}}^{\text{M46}} + x_{\text{Mg}}^{\text{M3}} + 3x_{\text{Mg}}^{\text{M46}})} \\ = \text{Fe}/(\text{Fe} + \text{Mg})_{\text{sa}},$$

$$y_{\text{sa}} = x_{\text{Al}}^{\text{T3}},$$

leading to the site-fractions:

$$x_{\text{Fe}}^{\text{M3}} = x_{\text{sa}}(1 - y_{\text{sa}}),$$

$$x_{\text{Mg}}^{\text{M3}} = (1 - x_{\text{sa}})(1 - y_{\text{sa}}),$$

$$x_{\text{Al}}^{\text{M3}} = y_{\text{sa}},$$

$$x_{\text{Fe}}^{\text{M46}} = x_{\text{sa}},$$

$$x_{\text{Mg}}^{\text{M46}} = 1 - x_{\text{sa}},$$

$$x_{\text{Al}}^{\text{T3}} = y_{\text{sa}},$$

$$x_{\text{Si}}^{\text{T3}} = 1 - y_{\text{sa}}.$$

The corresponding end-member proportions are:

$$p_{\text{spr4}} = 1 - y_{\text{sa}} - x_{\text{sa}}(1 - y_{\text{sa}}/4),$$

$$p_{\text{fspr}} = x_{\text{sa}}(1 - y_{\text{sa}}/4),$$

$$p_{\text{spr5}} = y_{\text{sa}}.$$

Ideal activity expressions for each end-member are:

$$a_{\text{spr4}} = \left(x_{\text{Mg}}^{\text{M3}}\right)^1 \left(x_{\text{Mg}}^{\text{M46}}\right)^3 \left(x_{\text{Si}}^{\text{T3}}\right)^1,$$

$$a_{\text{fspr}} = \left(x_{\text{Fe}}^{\text{M3}}\right)^1 \left(x_{\text{Fe}}^{\text{M46}}\right)^3 \left(x_{\text{Si}}^{\text{T3}}\right)^1,$$

$$a_{\text{spr5}} = \left(x_{\text{Al}}^{\text{M3}}\right)^1 \left(x_{\text{Mg}}^{\text{M46}}\right)^3 \left(x_{\text{Al}}^{\text{T3}}\right)^1.$$

Thermodynamic data for sapphirine end-members (Table 2) were derived by fitting the MAS experiments of Hollis & Harley (2003), in addition to the same end-member equilibria (Hensen, 1972; Newton, 1972; Doroshev & Malinovskiy, 1974; Seifert, 1974; Ackermann *et al.*, 1975; Waters, 1986) used to derive the Holland & Powell (1998) sapphirine model. In addition, composition data from natural examples of sapphirine-bearing mineral assemblages were used to calibrate the feldspar end-member.

Interaction energy parameters, W_{ij} , expressing non-ideal mixing, are not well-constrained by existing experimental data but are required for the calibration of thermodynamic data. Nevertheless,

Table 2. Thermodynamic properties of the phase end-members used for calculations and contained within the dataset tc323.txt. Definitions of thermodynamic properties are given in Holland & Powell (1998).

Phase and abbreviation	EM	H	$sd(H)$	S	V	a	b	c	d	a_1	a_2	K	K'	dK/dT	T_c	S_{max}	V_{max} (aq cp)
Biotite, bi	phl	-6218.73	3.21	328	14.964	0.7703	-3.6939	-2328.9	-6.5316	5.79	10	513	4	-0.0769			
	ann	-5151.65	3.45	418	15.432	0.8157	-3.4861	19.8	-7.4667	5.79	10	513	4	-0.0769			
	east	-6337.74	3.37	318	14.738	0.7855	-3.8031	-2130.3	-6.8937	5.79	10	513	4	-0.0769			
	obi	-5873.77	3.18	358	15.12	0.7854	-3.6246	-1546	-6.8433	5.79	10	513	4	-0.0769			
Garnet, g	py	-6284.35	1.32	266.3	11.318	0.6335	0	-5196.1	-4.3152	4.36	10	1737	4	-0.2605			
	alm	-5263.57	1.39	340	11.511	0.6773	0	-3772.7	-5.044	4.03	10	1690	4	-0.2535			
Sapphirine, sa	spr5	-11138.46	4.38	420	19.751	1.1755	-2.5416	-7508	-9.3364	4.9	10	1200	4	-0.18			
	spr4	-11003.38	3.49	450	19.905	1.1603	-2.4324	-7706.6	-8.9742	4.9	10	1200	4	-0.18			
	fspr	-9584.63	5.39	552	19.923	1.1329	-0.7348	-10420.2	-7.0366	4.9	10	1200	4	-0.18			
Orthopyroxene, opx	en	-3090.12	0.94	132.5	6.262	0.3562	-0.299	-596.9	-3.1853	5.05	10	1070	4	-0.1605			
	fs	-2388.71	0.95	190.6	6.592	0.3987	-0.6579	1290.1	-4.058	6.32	10	1010	4	-0.1515			
	mgts	-3189.38	0.82	131	5.9	0.3714	-0.4082	-398.4	-3.5471	5.08	10	1144	4	-0.1716			
	ofm	-2746.36	0.8	161.55	6.427	0.3774	-0.4785	346.6	-3.6217	5.7	10	1038	4	-0.1605			
	sp	-2301.23	0.97	81.5	3.978	0.2427	-0.6037	-2315.1	-1.6781	4.31	10	1945	4	-0.2918			
Spinel, sp	herc	-1959.03	0.98	107.5	4.075	0.2833	-0.5376	609.8	-2.7136	3.95	10	2120	4	-0.318			
	osm1	-14967.9	4.28	701	37.893	1.6258	-3.5548	-8063.5	-13.4909	0.76	10	810	4	-0.1215			
Osumilite, osm	osm2	-14809.71	4.7	724	38.44	1.6106	-3.4457	-8262.1	-13.1288	0.76	10	810	4	-0.1215			
	fosm	-14248.33	4.44	762	38.32	1.656	-3.4163	-6497.7	-14.1143	0.8	10	800	4	-0.12			
Cordierite, cd	crd	-9163.32	1.77	407.5	23.322	0.8213	4.3339	-8211.2	-5	0.76	10	810	4	-0.1215	1800	20	0.2
	ferd	-8436.08	1.81	475	23.71	0.8515	4.4724	-6645	-5.6234	0.76	10	810	4	-0.1215	1800	20	0.2
	herd	-9446.93	2.14	487.3	23.322	0.8697	5.1995	-7723.7	-5.2512	0.76	10	810	4	-0.1215	1800	20	0.2
	ql	-3683.6	1.52	66	10.56	0.33	0	0	0	-0.5	10	470	4	-0.0705			
Liquid, liq	kspL	-3992.77	3.09	129.5	11.468	0.3673	0	0	0	6	10	260	4	-0.039			
	silL	-4142.8	2.07	62.4	10.27	0.3802	0	0	0	1	10	300	4	-0.045			
	foL	-4465.14	1.56	-110	8.486	0.5358	0	0	0	14.5	10	730	4	-0.1095			
	faL	-2933.46	1.6	205	9.39	0.4794	0	0	0	16.9	10	410	4	-0.0615			
	h2oL	-295.71	0.1	45.5	1.414	0.08	0	0	0	108	10	40	4	-0.006			
	mu	-5984.16	3.21	292	14.083	0.7564	-1.984	-2170	-6.9792	5.96	10	490	4	-0.0735			
	cel	-5842.4	3.12	290	13.957	0.7412	-1.8748	-2368.8	-6.6169	5.96	10	700	4	-0.105			
	fecl	-5477.57	3.15	329	14.07	0.7563	-1.9147	-1586.1	-6.9287	5.96	10	700	4	-0.105			
K-feldspar	ksp	-3965.05	3.08	230	10.9	0.4488	-1.0075	-1007.3	-3.9731	3.35	10	574	4	-0.0861			
Sillimanite	sill	-2585.59	0.74	95.5	4.986	0.2802	-0.69	-1375.7	-2.3994	2.21	10	1320	4	-0.198	2200	4	0.035
Kyanite	ky	-2593.04	0.74	83.5	4.414	0.2794	-0.7124	-2055.6	-2.2894	4.04	10	1590	4	-0.2385			
Quartz	q	-910.88	0.37	41.5	2.269	0.1107	-0.5189	0	-1.1283	0.65	10	750	4	-0.1125	847	4.9	0.119
Free water	H ₂ O	-241.81	0.02	188.8	0	0.0401	0.8656	487.5	-0.2512	0	0	0	0	0			

the magnitude of energetics associated with Tschermak and Fe-Mg exchange in other minerals may provide a useful analogy for that of sapphirine. The interaction parameter $W_{spr4,spr5}$ conveys the energetics of Mg-Tschermak substitution in sapphirine, and by analogy with biotite is set at 10 kJ mol⁻¹. Fe-Mg mixing is assumed to involve 2 kJ per atom, similar in magnitude to other minerals (e.g. biotite and orthopyroxene), leading to $W_{spr4,fspr} = 8$ kJ mol⁻¹. The remaining W_{ij} term, $W_{fspr,spr5}$, is calculated at 12 kJ mol⁻¹ using the approach in Powell & Holland (1999), assuming that non-ideality in the Fe subsystem of sapphirine is identical to the Mg subsystem. The topology of sapphirine-bearing equilibria, in FMAS and KFMASH, is sensitive to the choice of W_{ij} values. The employed values of W result in a topology consistent with the accepted topological relationships between the FMAS and KFMASH systems (e.g. Audibert *et al.*, 1995), thus allowing practical calculations for natural, but low Fe³⁺, rock types involving sapphirine.

THERMOCALC tc323 has been used for the calculation of all the phase diagrams presented here, using the 27 January 2004 upgrade of the Holland & Powell (1998) internally consistent thermodynamic dataset (dataset filename tc323.txt). Thermodynamic data and datafile scripts for sapphirine and other phases used in calculations are provided in Table 2 and Appendix A respectively.

PHASE RELATIONS IN FMAS(H)

FMAS petrogenetic grids (e.g. Hensen, 1971; Hensen & Green, 1973; Harley, 1998a) have been the most widely used for the interpretation of the evolution of sapphirine-bearing assemblages (e.g. Harley, 1989, 1998b). Therefore it is initially instructive to compare our new calculations with existing published FMAS

grids. As discussed below, a comparison enables an evaluation of the applicability of FMAS grids to interpret the metamorphic evolution of a given diagnostic mineral assemblage. The P - T location of FMAS invariant points has been subject to some uncertainty over the past 30 years (e.g. Hensen & Green, 1971; Bertrand *et al.*, 1991; Harley, 1998a). A critical constraint is provided by topological and element partitioning arguments, namely that the FMAS invariant points must lie to lower pressure than the stable MAS invariant point [g sp] (e.g. Hensen, 1971; Newton, 1972; Newton *et al.*, 1974; Hensen & Harley, 1990; Fig. 1a; invariant points are named using absent-phase notation []). Experimental data, some of which are used to calibrate the current sapphirine model, constrains the [g sp] MAS invariant point to approximately 7.5–8 kbar (e.g. Newton, 1972; Newton *et al.*, 1974; Fig. 1a). Consequently the calculated FMAS invariant points lie at still lower pressure, calculated at around 6.5 kbar (and 950–1000 °C). However, our results contrast significantly with the preferred location of FMAS invariant points in the literature, which are located at around 8–11 kbar (Fig. 1c). The apparent discrepancy between our calculations, and the experiments that constrain the database on which our calculations are based, may be understood with reference to the influence of H₂O on FMAS equilibria.

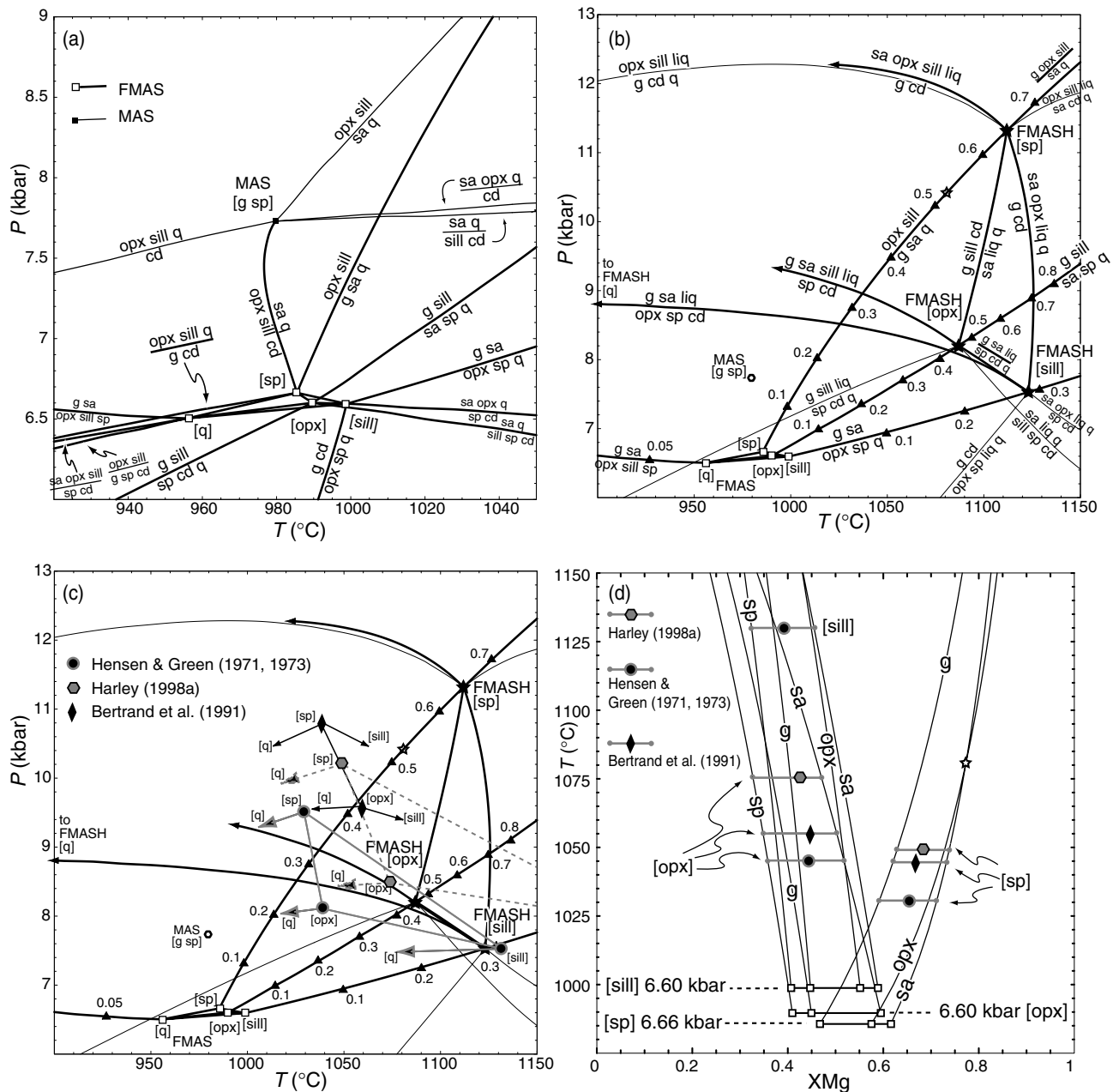


Fig. 1. P - T diagrams showing the relationship between calculated MAS, FMAS and FMASH subsystems and locations of experimentally and qualitatively derived petrogenetic grids. (a) location of FMAS equilibria (thick lines) with respect to MAS equilibria (thin lines). FMAS [q]-absent equilibria are shown for ease of comparison with Hensen & Green (1973) and Harley (1998a) grids. (b) Relationship of the dry FMAS equilibria from (a) to hydrous-melt-bearing FMASH equilibria. FMASH invariant points are located to higher temperatures along FMAS cordierite-absent (degenerate) univariant reactions. Numbered triangles along these cordierite-absent reactions denote $a_{\text{H}_2\text{O}}$, a proxy for the amount of water buffered by an assemblage. Each FMASH invariant point occurs at different $a_{\text{H}_2\text{O}}$, indicating the differing ability of FMAS assemblages to buffer H_2O . FMAS intersections [sp], [opx] and [sill] will 'slide' along the cordierite-absent univariant reactions from the true FMAS invariant points with increasing $a_{\text{H}_2\text{O}}$. Thus in a system in which the amount of H_2O is fixed, the P - T location of [sp], [opx] and [sill] intersections are thus determined by the corresponding $a_{\text{H}_2\text{O}}$. The quartz-absent FMASH invariant point, located at 622 $^{\circ}\text{C}$, is metastable with respect to corundum. (c) Experimentally and/or qualitatively and/or semi-quantitatively derived grids of three studies are superimposed onto the calculated equilibria of (b). The presence of impurities in the experimental charges do not allow for a determination of the P - T location of true (dry) FMAS equilibria. (d) T - X projection showing the changes in phase compositions along the three cordierite-absent FMAS univariant equilibria $\text{opx} + \text{sill} = \text{g} + \text{sa} + \text{q}$, $\text{g} + \text{sill} = \text{sa} + \text{sp} + \text{q}$ and $\text{g} + \text{sa} = \text{opx} + \text{sp} + \text{q}$ depicted in (a-c). Intersections [sp], [opx] and [sill] determined by Hensen & Green (1971, 1973) and Harley (1998a) are depicted to demonstrate the approximate phase compositions at their estimated FMAS invariant points/grids. Open star depicts a singularity between sapphirine and orthopyroxene. Open squares represent the composition of each phase at the calculated FMAS invariant points.

Figure 1(b,c) shows that varying amounts of H₂O, manifest as an assemblage-buffered $a_{\text{H}_2\text{O}}$, results in the migration of FMAS intersections [sp], [opx] and [sill] along cordierite-absent reactions until hydrous melt is introduced at FMASH invariant points (analogous to the argument in Powell & Sandiford, 1988, relating to a_{O_2}). Therefore, crucially, the amount of water in experimental charges used to determine the P - T location of so-called FMAS invariant points (e.g. Hensen & Green, 1971, 1973; Bertrand *et al.*, 1991) is a primary control on the P - T position of the resulting entire 'FMAS' grid. This is hardly surprising given that cordierite is a hydrous phase. Given that H₂O is typically not the only variable impurity in experimental charges, differences in the well-located P - T location of 'FMAS' equilibria between studies may be understood by also considering other impurities (e.g. Na₂O, K₂O). It is likely that the small amount of melt produced in the experiments mops up the small amount of available Na₂O, K₂O and so on, as well as H₂O, effectively buffering the $a_{\text{H}_2\text{O}}$ in the experimental charges, and buffering $a_{\text{H}_2\text{O}}$ in a reproducible way. For example, increasing $a_{\text{H}_2\text{O}}$ leads to a melt-bearing invariant point along (sp cd) at $a_{\text{H}_2\text{O}} = 0.65$ in FMASH (Fig. 1b,c), whereas in the presence of sufficient K₂O to stabilize osumilite in KFMASH, the melt-bearing invariant point occurs at $a_{\text{H}_2\text{O}} = 0.15$. For less K₂O, in the presence of melt, $a_{\text{H}_2\text{O}}$ may therefore lie between 0.15 and 0.65, corresponding to a pressure range from 7.6 to 11.3 kbar. Importantly, although there is insufficient information in terms of minor constituents, and particularly H₂O, in the experiments, the meaning of the experimental results can be understood in terms of $a_{\text{H}_2\text{O}}$, this being buffered by the melt coexisting with the minerals. Thus, the experimentally derived FMAS grids are more properly akin to constant $a_{\text{H}_2\text{O}}$ sections of the system FMASH, applicable at a particular $a_{\text{H}_2\text{O}}$.

Figure 1(c) shows that the (invariant) points of the Hensen & Green (1973) and Harley (1998a) grids lie close to the locus of the calculated cordierite-absent FMAS univariant reactions, and further suggest those grids to be associated with $a_{\text{H}_2\text{O}}$ approximately 0.3–0.35 and 0.4–0.5 respectively. The fit between calculated cordierite-absent FMAS univariant reactions and the experimental results of Bertrand *et al.* (1991) appear to be worse; however, there is considerable uncertainty in the pressure locations of their invariant points (see their fig. 3). The effect of other components (e.g. CaO, Fe₂O₃) on the results of experiments may contribute to the imperfect fit of experimentally derived grids onto the locus of calculated cordierite-absent FMAS univariant reactions.

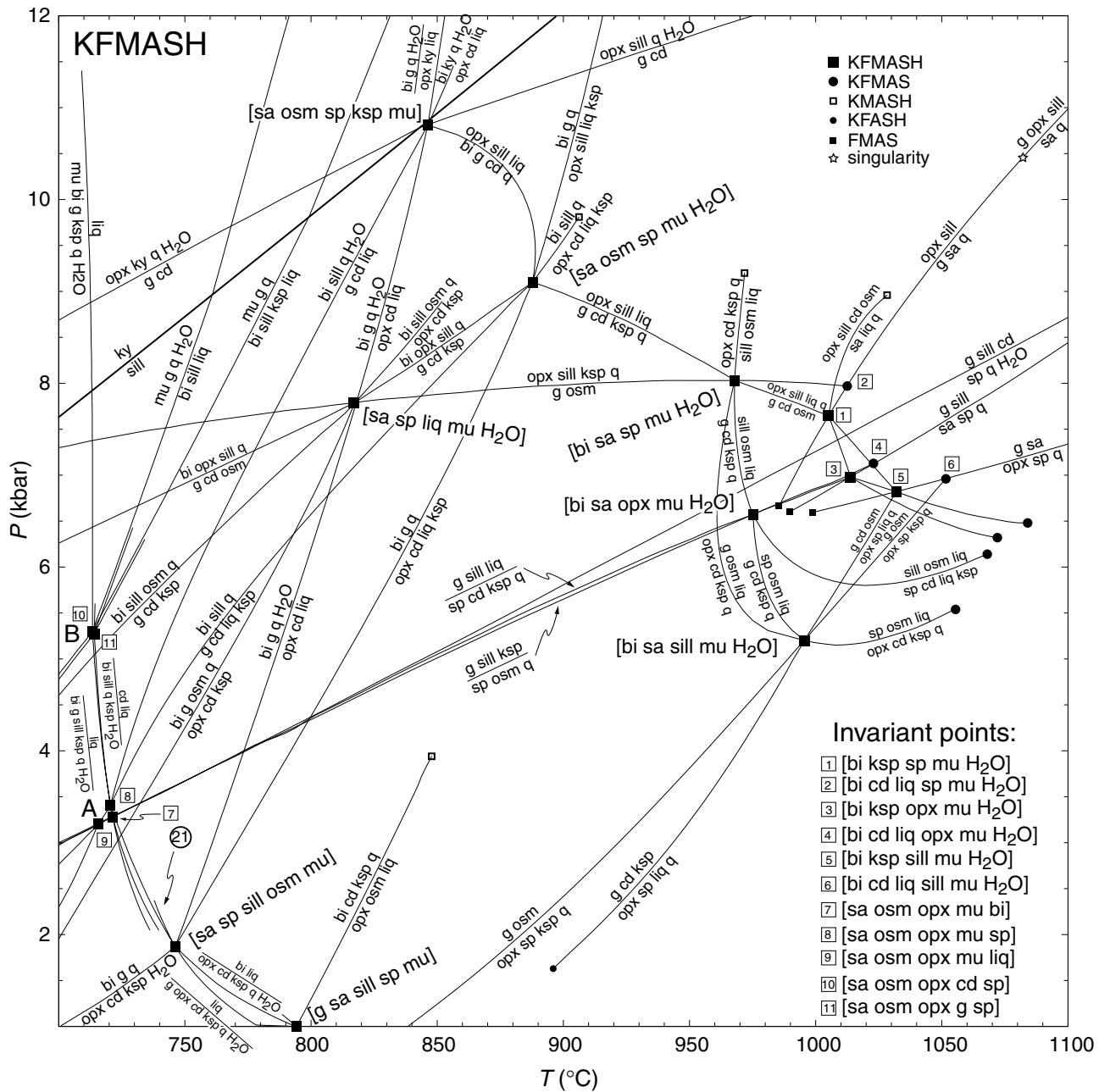
The composition of phases that may be expected at the locations of the experimentally constrained and semi-quantitative invariant points (Hensen & Green, 1971, 1973; Bertrand *et al.*, 1991; Harley, 1998a) are shown in Fig. 1d, and at least for the [opx] and [sill] intersections, do not differ greatly [i.e. $< 0.1X_{\text{Mg}}$, where $X_{\text{Mg}} = 1 - \text{Fe}/(\text{Fe} + \text{Mg})$] from the calculated

FMAS invariant point compositions. In contrast, compositions along the cordierite-spinel absent univariant become markedly more magnesian up-temperature, such that the compositions of phases at experimentally constrained and semi-quantitative [sp] invariant points may be $\geq 0.1X_{\text{Mg}}$ different from the calculated FMAS [sp] point composition. Importantly, the compositions of phases reported by Bertrand *et al.* (1991) in the vicinity of their [sp] intersection are closely consistent with the compositions of phases shown on Fig. 1d at about 1050–1100 °C.

Although the above discussion does not provide a validation of the sapphirine model presented here, the FMAS mineral equilibria are shown to be placed in an appropriate position with respect to the well-located MAS equilibria. Moreover this discussion shows why the calculated FMAS grid is displaced by 2 or 3 kbar down pressure, for example, with respect to the currently accepted FMAS grids in the literature. As the FMAS system does not incorporate essential rock-forming components such as K₂O and H₂O, thereby disallowing the consideration of assemblages containing biotite, K-feldspar, osumilite and silicate melt, the remainder of calculations will be performed within the KFMASH system.

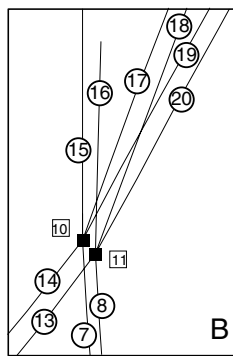
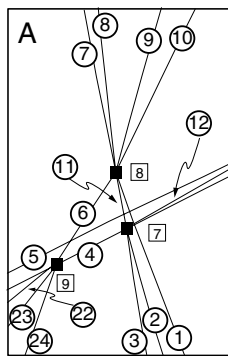
THE KFMASH PETROGENETIC GRID

The P - T projection (Fig. 2) depicts the univariant and invariant phase relations for all bulk compositions for the KFMASH system that involve quartz. The topology of the grid in Fig. 2 to temperatures lower than about 960 °C is similar to that presented in White *et al.* (2001), except for the inclusion of osumilite ± biotite-bearing equilibria. The lower temperature equilibria will not be discussed further here. Above 960 °C a cluster of invariant points involving sapphirine and/or osumilite occur (Figs 2 & 3). The P - T location of these clustered invariant points is controlled by the position of the shallow dP/dT $g + cd + ksp + q = opx + sill + liq$ univariant reaction, defined experimentally by Carrington & Harley (1995a), and previously calibrated into the dataset for White *et al.* (2001). The location of KFMASH invariant points are also controlled by the locus of the previously discussed cordierite-liquid-absent FMAS equilibria that are degenerate in KFMASH. The topology of the osumilite- and sapphirine-bearing invariant points [bi sa sp], [bi ksp sp] and [bi cd liq sp] (Fig. 3) is identical to that predicted experimentally by Audibert *et al.* (1995). Moreover, the clusters of KFMASH [sp]-, [opx]- and [sill]-invariant points define the same 'triangular' topology as that proposed for the melt-absent FMAS system (compare Figs 1 & 3; Hensen, 1971). Signs of reaction coefficients for the calculated KFMASH univariant reactions are in agreement with experimental and/or qualitative predictions (e.g. Hensen, 1971; Audibert *et al.*, 1995; Figs 1 & 3). The KFMASH [sill]- and [opx]-invariant points and



Invariant points:

- 1 [bi ksp sp mu H₂O]
- 2 [bi cd liq sp mu H₂O]
- 3 [bi ksp opx mu H₂O]
- 4 [bi cd liq opx mu H₂O]
- 5 [bi ksp sill mu H₂O]
- 6 [bi cd liq sill mu H₂O]
- 7 [sa osm opx mu bi]
- 8 [sa osm opx mu sp]
- 9 [sa osm opx mu liq]
- 10 [sa osm opx cd sp]
- 11 [sa osm opx g sp]



- 12 g + cd + ksp + q + H₂O = bi + liq
- 13 mu + q = bi + sill + cd + ksp + H₂O
- 14 mu + g + q = bi + sill + ksp + H₂O
- 15 mu + bi + g + ksp + q + H₂O = liq
- 16 mu + bi + ksp + q + H₂O = cd + liq
- 17 mu + g + q + H₂O = bi + sill + liq
- 18 mu + q + H₂O = bi + sill + cd + liq
- 19 mu + g + q = bi + sill + liq + ksp
- 20 mu + q = bi + sill + cd + liq + ksp
- 21 bi + g + ksp + q + H₂O = opx + liq
- 22 bi + g + sill = sp + ksp + q + H₂O
- 23 bi + sill + q = sp + cd + ksp + H₂O
- 24 bi + sp + q = g + cd + ksp + H₂O

CV	[bi ksp sp]	[bi ksp opx]	[bi ksp sill]	FMAS [sp]	FMAS [opx]	FMAS [sill]
	7.65 kbar, 1005.1 °C	6.98 kbar, 1013.8 °C	6.82 kbar, 1031.9 °C	6.66 kbar, 985.5 °C	6.60 kbar, 989.7 °C	6.60 kbar, 998.9 °C
1 - x_{sa}	0.67	0.56	0.56	0.61	0.59	0.59
y_{sa}	0.27	0.29	0.28	0.28	0.28	0.28
1 - x_{opx}	0.64	—	0.53	0.57	—	0.55
y_{opx}	0.25	—	0.28	0.26	—	0.27
1 - x_{osm}	0.80	0.73	0.73	—	—	—
y_{osm}	0.18	0.17	0.18	—	—	—
1 - x_g	0.53	0.43	0.43	0.47	0.45	0.45
1 - x_{cd}	0.80	0.72	0.72	0.76	0.74	0.74
h_{cd}	0.25	0.15	0.10	—	—	—
1 - x_{sp}	—	0.39	0.39	—	0.41	0.41
q_{Liq}	0.29	0.30	0.31	—	—	—
fsp_{Liq}	0.44	0.45	0.45	—	—	—
ol_{Liq}	0.017	0.024	0.031	—	—	—
1 - x_{Liq}	0.40	0.32	0.31	—	—	—
$h2o_{Liq}$	0.19	0.14	0.11	—	—	—

Table 3. Compositions of the phases at the three sapphirine-quartz-bearing KFMASH invariant points. $x_k = \text{Fe}/(\text{Fe} + \text{Mg})$, thus $1 - x_k = X_{\text{Mg}}(k)$; $y_{\text{opx}} = X_{\text{Al}}^{\text{M1}}$; $y_{\text{osm}} = 3 - 3X_{\text{Al}}^{\text{T1}}$; h is $X_{\text{H}_2\text{O}}^{\text{hydr}}/X_{\text{H}_2\text{O}}$; $q_{\text{Liq}}, fsp_{\text{Liq}}, ol_{\text{Liq}}$ and $h2o_{\text{Liq}}$ are proportions of silica SiO_2 , K-feldspar KAlSi_3O_8 , olivine $(\text{Fe}, \text{Mg})_2\text{SiO}_4$ and water H_2O end-members in the liquid, respectively. The values of $y_{sa} = X_{\text{Al}}^{\text{M3}}$ correspond to a sapphirine between the commonly stated 2:2:1 and 7:9:3 end-members. KFMASH X_{Mg} increases in the order liquid, spinel, garnet, orthopyroxene, sapphirine, cordierite, osmilitite. CV = composition variable.

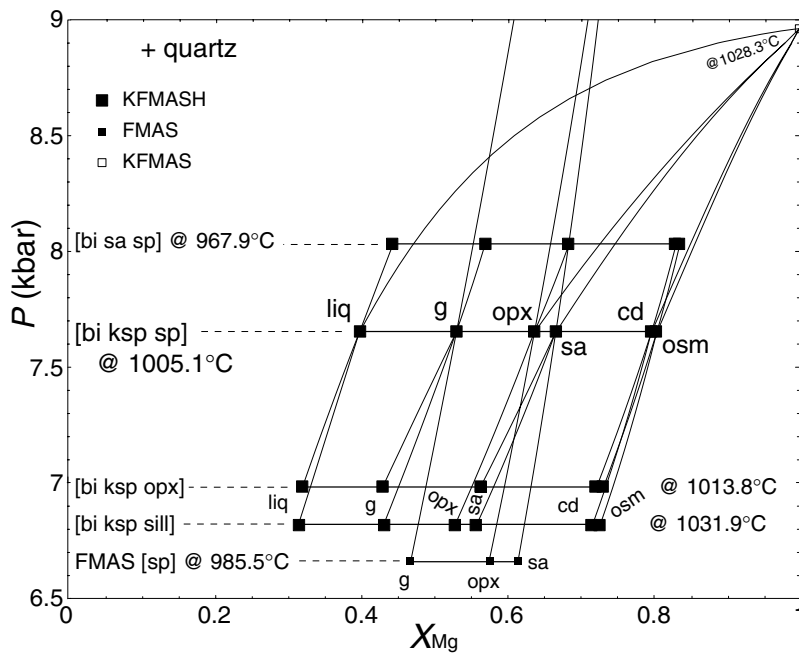


Fig. 4. P - X projection depicting the composition of phases at the KFMASH invariant points [bi ksp sp], [bi ksp opx] and [bi ksp sill]. Phase compositions along univariant reactions emanating from [bi ksp sp] are also shown. All phases become increasingly magnesian with increasing pressure. The univariant reaction $\text{opx} + \text{sill} + \text{cd} + \text{osm} = \text{sa} + \text{liq} + \text{q}$ terminates in KFMASH ($X_{\text{Mg}} = 1.0$). Squares represent the composition of each phase at the calculated KFMASH and FMAS invariant points.

due to the presence of a singularity along the degenerate KFMASH univariant reaction involving garnet + sapphirine + orthopyroxene + sillimanite + quartz (Figs 1d & 2). The relative similarity in calculated X_{Mg} of sapphirine and orthopyroxene at pressures above and below the singularity implies the stable coexistence of (K)FMAS(H) sapphirine + orthopyroxene + sillimanite + quartz assemblages is restricted, corroborating the findings of Bertrand *et al.* (1991) and Audibert *et al.* (1995). Since Fe^{3+} preferentially partitions into sapphirine over orthopyroxene (e.g. Sandiford *et al.*, 1987), the calculated difference between x_{sa} and x_{opx} at $P < 10.42$ kbar is anticipated to expand in the system KFMASHO, thus 'pushing' the singularity further up-pressure (or even out of existence).

In contrast to x_{sa} , y_{sa} shows little variation over the P - T range covered by the calculated quartz-bearing

invariant points, with the y_{sa} values in Table 3 lying between the commonly stated 2:2:1 ($y_{sa} = 0$) and 7:9:3 ($y_{sa} = 0.5$) sapphirine end-members for natural occurrences. Limited variability in the alumina-content of sapphirine is also noted for quartz-bearing MAS and FMASH(O) experiments (Bertrand *et al.*, 1991; Hollis & Harley, 2003), in which sapphirine composition has been monitored with changing P - T . Nevertheless, the absence of systematic sapphirine composition data from all but the experiments of Hollis & Harley (2003) used to calibrate the thermodynamic model implies that tight constraints on the variability and magnitude of both x_{sa} and y_{sa} with P , T and X are lacking.

The signs of the slopes (dP/dT) and locus of most univariant reactions calculated by THERMOCALC are consistent with those suggested experimentally by Audibert *et al.* (1995) and experimentally and qualitatively by Carrington & Harley (1995a). The

exception is the garnet-absent univariant reaction $opx + sill + cd + osm = sa + liq + q$ (KFMASH), calculated with positive and curved dP/dT in THERMOCALC (Figs 2 & 3), but interpreted to have a negative dP/dT by Audibert *et al.* (1995). The curved nature of the calculated univariant reaction is related to Tschermaks substitution between sapphirine and orthopyroxene.

The P - T location of the [bi sa sp] invariant point, as proposed by Carrington & Harley (1995a) at about 7.7 kbar and 940 °C, compares well with the THERMOCALC-calculated position of about 8 kbar and 960 °C. In contrast, a larger temperature difference exists for the location of the [bi ksp sp] invariant point (Figs 2 & 3) marking the introduction of sapphirine-quartz-bearing assemblages. Whereas Audibert *et al.* (1995) place [bi ksp sp] at about 1050 °C, calculations by THERMOCALC place [bi ksp sp] at approximately 1005 °C (Table 3). A useful exercise in assessing whether this temperature discrepancy is reconcilable is to compare directly the P - T locations of assemblage fields on calculated pseudosections with experimentally determined assemblages. In this way, the applicability of the sapphirine a - x model may be tested for consistency with experimental mineral assemblage relationships. As sapphirine was not produced in the experiments of Carrington & Harley (1995a,b), a result of the maximum temperature for their experiments being 1000 °C at pressure intervals of ≥ 1 kbar, the following pseudosections are calculated only for experimental bulk compositions in Audibert *et al.* (1995).

PSEUDOSECTIONS FOR KFMASH EXPERIMENTS

P - T pseudosections calculated using the bulk compositions M2 and M3 of Audibert *et al.* (1995) are presented in Fig. 5. The water content used to calculate the P - T pseudosections has been assumed to be small (Fig. 5), and is supported by the authors' statement that the proportion of liquid is minor, and that K-feldspar did not break down until ≥ 1050 °C (see Fig. 5). Less water in the bulk composition will stabilize K-feldspar further up-temperature, whereas greater amounts of water will restrict K-feldspar to lower temperatures in favour of silicate melt and/or cordierite at higher temperatures (e.g. Kelsey *et al.*, 2003b). A systematic pressure difference of around 2 kbar between the experimental results of Carrington & Harley (1995a) and Audibert *et al.* (1995) was attributed by Carrington & Harley (1995b) to an incorrect friction correction in the experiments of Audibert *et al.* (1995). The pressures determined for [bi sa sp], [bi ksp sp] (both KFMASH) and [bi cd liq sp] (KFMAS) by THERMOCALC are consistent with the experimental results of Carrington & Harley (1995a), at around 7.5–8 kbar for the cluster of invariant points. Following Carrington & Harley (1995b), the pressures of Audibert *et al.* (1995) are reduced by

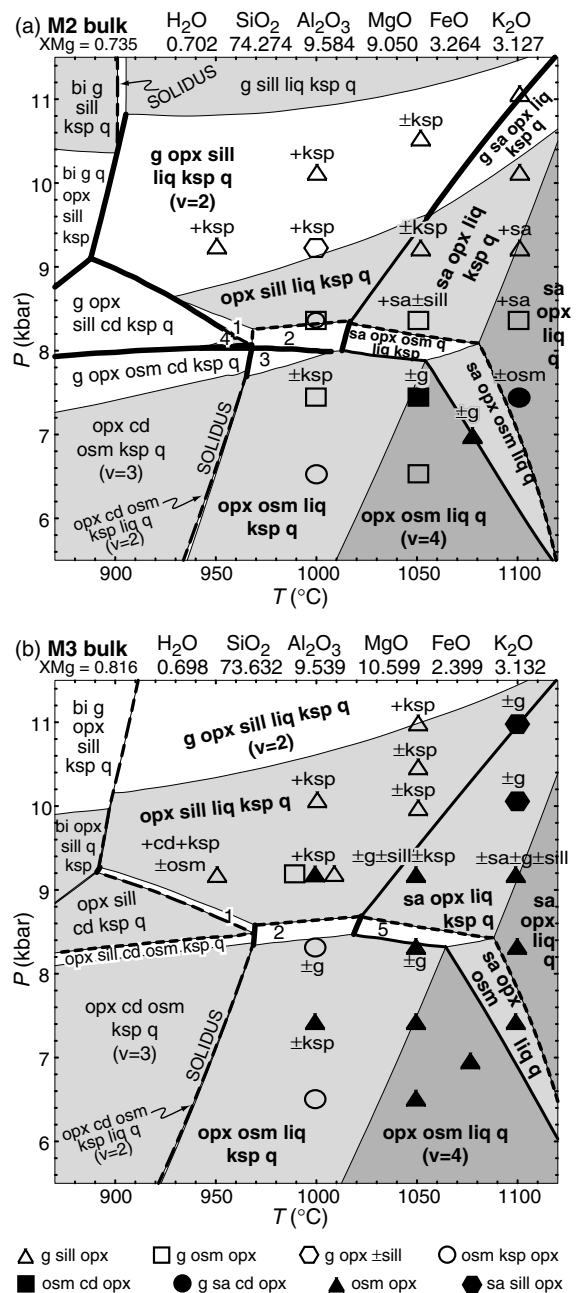


Fig. 5. P - T pseudosections calculated for bulk compositions M2 (a) and M3 (b) of Audibert *et al.* (1995). Water content of the bulk compositions is assumed as low, restricting cordierite stability in favour of liquid/melt. Superimposed on the pseudosections are the experimental results of Audibert *et al.* (1995), with pressures adjusted according to Carrington & Harley (1995b). Some fields are labelled in bold to distinguish them from experimental results. Sapphirine stabilizes above 1010 °C. Osumilite-sapphirine-bearing assemblages are favoured at pressures below about 8 kbar and extreme temperatures. Bold, fine-dashed, coarse-dashed and thick bold lines delineate sapphirine and osumilite stability, the solidus and univariant reactions respectively. Variance, v , of fields as indicated. Labelled fields: 1, $opx + sill + cd + liq + ksp + q$; 2, $opx + sill + osm + liq + ksp + q$; 3, $g + opx + osm + liq + ksp + q$; 4, $opx + sill + cd + ksp + q$; 5, $sa + opx + osm + liq + ksp + q$.

2 kbar for comparison with the calculated P - T pseudosections.

Assuming that a relative 1 kbar change in THERMOCALC is equivalent to that in the experiments of Audibert *et al.* (1995), the fit of calculated fields with the experimentally determined assemblages is generally good (Fig. 5). An imperfect fit between experiments and calculations could be attributed to many factors, including: (i) sluggish reaction rates in Mg-rich compositions, resulting in the persistence of reactants amongst products in the experiments (Audibert *et al.*, 1995); (ii) small amounts of Ca and Na in garnet and osumilite experiment seeds respectively; (iii) water content affecting cordierite stability; (iv) the effect of Fe^{3+} ; (v) P - T uncertainty on thermodynamically calculated field boundaries; and (vi) uncertainty relating to the 2 kbar correction advocated by Carington & Harley (1995b). Points (i) and (ii) above may be manifest where Audibert *et al.* (1995) commonly indicate that garnet and/or osumilite comprise part of an equilibrium assemblage, commonly well outside the stability suggested by calculations. Garnet in particular has a reasonably poor fit with the calculated M3 pseudosection (Fig. 5b). Thus it is possible that garnet and osumilite seeds have persisted metastably. This is supported by (re)equilibration problems manifest as strongly zoned garnet, with cores un-reset from seed compositions (Audibert *et al.*, 1995). In addition, the presence of Ca and Na in experimental seeds may enhance the stability range of garnet and osumilite. In particular, Ca-bearing garnet present in the experiments may be stabilized down-pressure with respect to Ca-absent garnet used in the calculations. Problems with equilibration during experimental runs were also noted for sapphirine (see also Bertrand *et al.*, 1991; Hollis & Harley, 2003). The presence of cordierite in some experimental runs may indicate bulk water content is higher than that used in calculations. However, Audibert *et al.* (1995) stated that cordierite and osumilite were difficult to detect in experimental run products.

Nevertheless, the sequence of mineral assemblage changes predicted up-pressure in the experimental runs is consistent with the pseudosection calculations, including those assemblages involving sapphirine. For example, osumilite-bearing assemblages at lower pressures yield to sillimanite- and/or sapphirine-bearing assemblages at higher pressures, depending on temperature, with the P - T stability of garnet-bearing assemblages determined by the X_{Mg} of the bulk composition. Audibert *et al.* (1995) deduced that sapphirine + osumilite assemblages are restricted to lower pressures than sapphirine + sillimanite assemblages, a conclusion matched by our calculations (Fig. 5). The equilibrium coexistence of sapphirine and quartz with sillimanite in the presence of liquid occurs in a narrow field related to the (degenerate KFMASH) FMAS univariant reaction $g + \text{opx} + \text{sill} = \text{sa} + \text{q}$ (see Fig. 3; Bertrand *et al.*, 1991).

Sapphirine is restricted to temperatures greater than approximately 1010 °C in the calculations, and will not occur stably to pressures approximately <8 kbar (Fig. 5) until temperatures exceed about 1050 °C for these bulk compositions. The direct comparison of calculated fields with experimental assemblages cannot unequivocally reconcile the approximate 40 °C discrepancy regarding the introduction of sapphirine + quartz. However, the experimental results of Audibert *et al.* (1995) do not exclude the possibility that sapphirine-quartz-bearing assemblages can form at temperatures lower than 1050 °C, since experiments were not undertaken in the temperature interval 1000–1050 °C. Furthermore, calculations indicate that sapphirine + quartz stability expands up-temperature from a wedge-shaped termination at around 1010 °C (Fig. 5), which could easily be missed in experimental runs (e.g. due to kinetics, equilibration problems or pressure interval of experiments). The stability fields of sapphirine and osumilite in the presence of quartz and liquid are calculated to overlap in P - T - X space, as determined by Audibert *et al.* (1995).

Mineral assemblage relationships not involving sapphirine are also of interest with regard to the interpretations of Audibert *et al.* (1995) and natural assemblages. Calculated osumilite stability is restricted to pressures less than approximately 8.7 kbar for the investigated bulk compositions. Additionally, the P - T - X extent of garnet-osumilite-bearing equilibria is calculated as less extensive than deduced experimentally, perhaps as a result of the metastable persistence of garnet and/or osumilite in experiments or the expanded stability of these minerals due to the presence of non-KFMASH components. Calculations suggest that the assemblage osumilite + orthopyroxene + sillimanite + K-feldspar + quartz (+ liquid) has a greater compositional stability range than garnet + osumilite (Fig. 5), in contrast to Audibert *et al.* (1995). Development of orthopyroxene + cordierite + K-feldspar + quartz symplectites after osumilite (e.g. Berg & Wheeler, 1976; Grew, 1982; Lal *et al.*, 1987; Arima & Gower, 1991; Audibert *et al.*, 1993) correspond to the crossing of the KFMASH solidus (and associated divariant field, $v = 2$) with decreasing temperature (Fig. 5). Orthopyroxene-sillimanite-quartz-bearing assemblages are determined both experimentally and thermodynamically to occur at lower temperatures and/or higher pressures than sapphirine-bearing equilibria, a feature recognized in natural examples and a texture commonly attributed to isobaric cooling (e.g. Morse & Talley, 1971; Ellis *et al.*, 1980; Grew, 1982; Sandiford, 1985; Lal *et al.*, 1987; Currie & Gittins, 1988; Kamineni & Rao, 1988; Sengupta *et al.*, 1990; Baba, 1999; Bose *et al.*, 2000).

Although the pseudosections presented in Fig. 5 cover a limited range of bulk composition, the assemblages and assemblage topology depicted on

these pseudosections account for many natural sapphirine-quartz-bearing assemblages (e.g. Ellis *et al.*, 1980; Grew, 1980, 1982; Kamineni & Rao, 1988; Motoyoshi & Hensen, 1989; Bertrand *et al.*, 1992; Guiraud *et al.*, 1996; Harley & Motoyoshi, 2000). Presumably, other sapphirine-quartz-bearing assemblages that are inconsistent with these pseudosections (e.g. sapphirine + osumilite + sillimanite + quartz; sapphirine + garnet + osumilite + quartz; sapphirine + sillimanite + garnet + osumilite + quartz; Ellis *et al.*, 1980) reflect different KFMASH bulk compositions and/or the effect of additional chemical components (e.g. Fe₂O₃, Na₂O). Without being able to account thermodynamically for the effects of these additional components on the stability of sapphirine and osumilite, the absolute temperature effects are unquantifiable. However, the observation that assemblages that contain a substantial amount of Fe³⁺ (for example) are reproducible in the KFMASH system (e.g. sapphirine + orthopyroxene + sillimanite + quartz; Guiraud *et al.*, 1996) suggests that the effect of additional components on *topological* relationships may be relatively small, at least for spinel-absent assemblages.

Given the relatively good fit between the limited experimental data and calculated pseudosections, plus the corroboration with natural assemblage and composition data, the new *a-x* model and thermodynamic data for sapphirine are believed to be appropriate for mineral calculations, here in quartz-bearing systems. Thus, further calculations applying the sapphirine model to investigate the *P-T-X* stability limits of sapphirine-quartz-bearing assemblages, and to investigate natural assemblage evolution with pseudosections, are warranted.

***P-T-X* STABILITY OF SAPPHIRINE-QUARTZ-BEARING ASSEMBLAGES**

Sapphirine-bearing assemblages were present in all of the aluminous experimental bulk compositions of Audibert *et al.* (1995). Likely composition constraints on the stability of KFMASH sapphirine are X_{Mg} and bulk alumina [A/AFM = Al₂O₃/(Al₂O₃ + FeO + MgO)]. *T-X*, *P-X* and *P-T* pseudosections are presented to illustrate general composition constraints on sapphirine stability (Figs 6–8).

The chosen bulk composition trends for *T-X* and *P-X* pseudosections are indicated along the *x*-axis of the pseudosections, Figs 6 & 7, and are adapted from the experimental bulk compositions of Carrington & Harley (1995a). The *P-T* pseudosections, Fig. 8, are calculated for two different A/AFM and different X_{Mg} values depicted as dashed vertical lines on the *T-X* and *P-X* pseudosections.

Common granulite facies assemblages such as garnet + orthopyroxene (Figs 6a & 7a) and garnet + sillimanite (Figs 6b & 7b) typically occur in compositions more iron-rich than about $X_{Mg} = 0.50$. How-

ever, such assemblages may also occur in more magnesian rocks at more elevated pressures (e.g. Fig. 8c). Sapphirine stability is generally favoured by more Mg-rich compositions (e.g. $X_{Mg} > 0.50$; Figs 6a & 7a). However, sapphirine may occur in more Fe-rich compositions (i.e. $X_{Mg} \leq 0.50$) if there is sufficient alumina (e.g. Figs 6b & 7b). Nevertheless, Fig. 8a shows that sapphirine stability is much restricted in aluminous compositions with $X_{Mg} \leq 0.50$, in this case being stable over a limited pressure and temperature range of only around 1 kbar and 100 °C. Sapphirine-orthopyroxene-quartz-bearing assemblages cover a relatively wide range of *P-T-X* space (Figs 5–8), indicating that this mineral association is probably the most common sapphirine-quartz-bearing assemblage. Indeed, orthopyroxene-bearing sapphirine-quartz assemblages occur in the majority of sapphirine + quartz terranes (Morse & Talley, 1971; Leong & Moore, 1972; Caporuscio & Morse, 1978; Ellis *et al.*, 1980; Grew, 1980, 1982; Perchuk *et al.*, 1985; Sandiford, 1985; Lal *et al.*, 1987; Sandiford *et al.*, 1987; Currie & Gittins, 1988; Kamineni & Rao, 1988; Motoyoshi & Hensen, 1989; Sengupta *et al.*, 1990; Bertrand *et al.*, 1992; Guiraud *et al.*, 1996; Ouzegane & Boumaza, 1996; Baba, 1999; Bose *et al.*, 2000). In contrast, sapphirine + sillimanite, sapphirine + garnet and sapphirine + osumilite assemblages have narrower *P-T-X* stability ranges. Hence these latter assemblages may be more useful for constraining peak metamorphic conditions, particularly if they also contain orthopyroxene (e.g. Kelsey *et al.*, 2003a,b).

Garnet-bearing assemblages occur in more Fe-rich compositions (and/or pressures >9–10 kbar), whereas osumilite occurs in more Mg-rich compositions (Figs 6–8). The extent of overlap between sapphirine-quartz stability with garnet and osumilite for a given A/AFM is dependent on the X_{Mg} . Coexisting garnet, sapphirine and quartz require sufficiently aluminous and Fe-rich compositions (e.g. A/AFM > 0.45, $X_{Mg} < 0.65$; Figs 6–8) whereas coexisting sapphirine, osumilite and quartz require sufficiently aluminous and magnesian compositions [e.g. A/AFM > 0.30–0.40 (approximately), $X_{Mg} > 0.70$; Figs 6–8].

In general, the minimum pressure at which sapphirine + quartz stabilizes increases with increasing X_{Mg} (Figs 6–8). Ultimately, the stability range of sapphirine in ferrous and magnesian compositions may only barely overlap (compare Fig. 8a & d which have the same A/AFM). Whereas the low temperature limit of sapphirine + quartz stability is typically controlled by the location of the narrow sa + q + sill ± opx ± g field (Figs 6 & 8) and is therefore relatively tightly constrained in *P-T* space for a given composition, the low pressure bound on sapphirine + quartz stability is typically controlled by the coexistence with cordierite (Figs 7 & 8). Due to problems in estimating the water content of

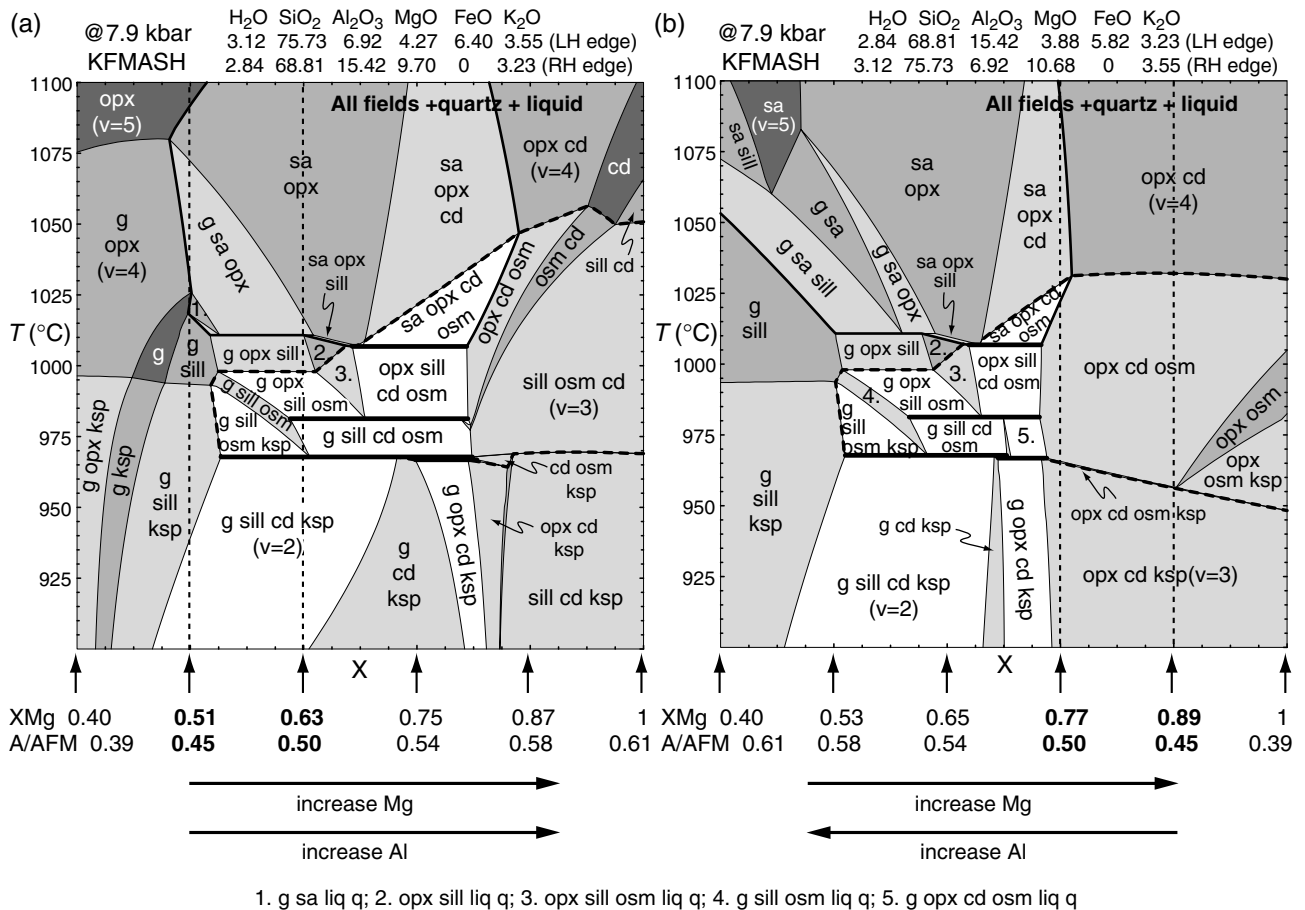


Fig. 6. T - X pseudosections calculated at 7.9 kbar for bulk compositions with varying alumina and iron-magnesium, given by the compositions (mol.%) above pseudosections. In highly magnesian compositions [right-hand side of (a) and (b)], sapphirine-bearing assemblages stabilize at pressures higher than 7.9 kbar. Only more iron-rich bulk compositions (e.g. X_{Mg} 0.40–0.85) allow for sapphirine-quartz stability as low as 7.9 kbar. The effect of bulk alumina is evident at the left-hand side of each pseudosection, with orthopyroxene stable at lower alumina (a), and sillimanite and/or sapphirine stable at higher alumina (b). Garnet + osumilite + quartz assemblages have stable range over approximately 0.25 X_{Mg} . Vertical dashed lines indicate compositions at which P - T pseudosections (Fig. 8) are calculated. Other bold, dashed and thick bold lines delineate sapphirine and osumilite stability and univariant reactions respectively. Variance, v , of fields as indicated.

cordierite occurring in natural assemblages, this boundary may be less accurately determinable.

Sapphirine + quartz stability is controlled by both bulk alumina and bulk X_{Mg} . Specifically, sapphirine + quartz can stabilize over a wide range of X_{Mg} depending on bulk alumina. However, due to the dependence on alumina it is not possible to explicitly state the minimum X_{Mg} required to stabilize sapphirine + quartz. Instead, it is apparent that sapphirine + quartz stability does not require highly magnesian bulk compositions. Nevertheless, in extending this conclusion to real rocks, which are not restricted to KFMASH, spinel, stabilized by components such as Fe_2O_3 , ZnO , Cr_2O_3 , is likely to enter more Fe-rich assemblages and hence affect the topology of sapphirine + quartz stability in such rocks.

P - T AND TEXTURAL EVOLUTION OF SAPPHIRINE + QUARTZ ASSEMBLAGES

P - T pseudosections depicted in Fig. 8 may also be used to investigate the textural evolution within sapphirine-quartz granulites in general, and are broadly applied to the evolution of natural low- Fe_2O_3 occurrences, such as the Napier Complex in Enderby Land, Antarctica. A more rigorous appraisal of the specific P - T evolution of sapphirine-quartz-bearing (and other) mineral assemblages from these terranes would require detailed information for individual mineral assemblages and reaction textures, such as petrography, mineral proportions, mineral compositions and bulk chemical composition.

It is first instructive to compare the topology of pseudosections in Fig. 8 (also Figs 6 & 7) with the uni-

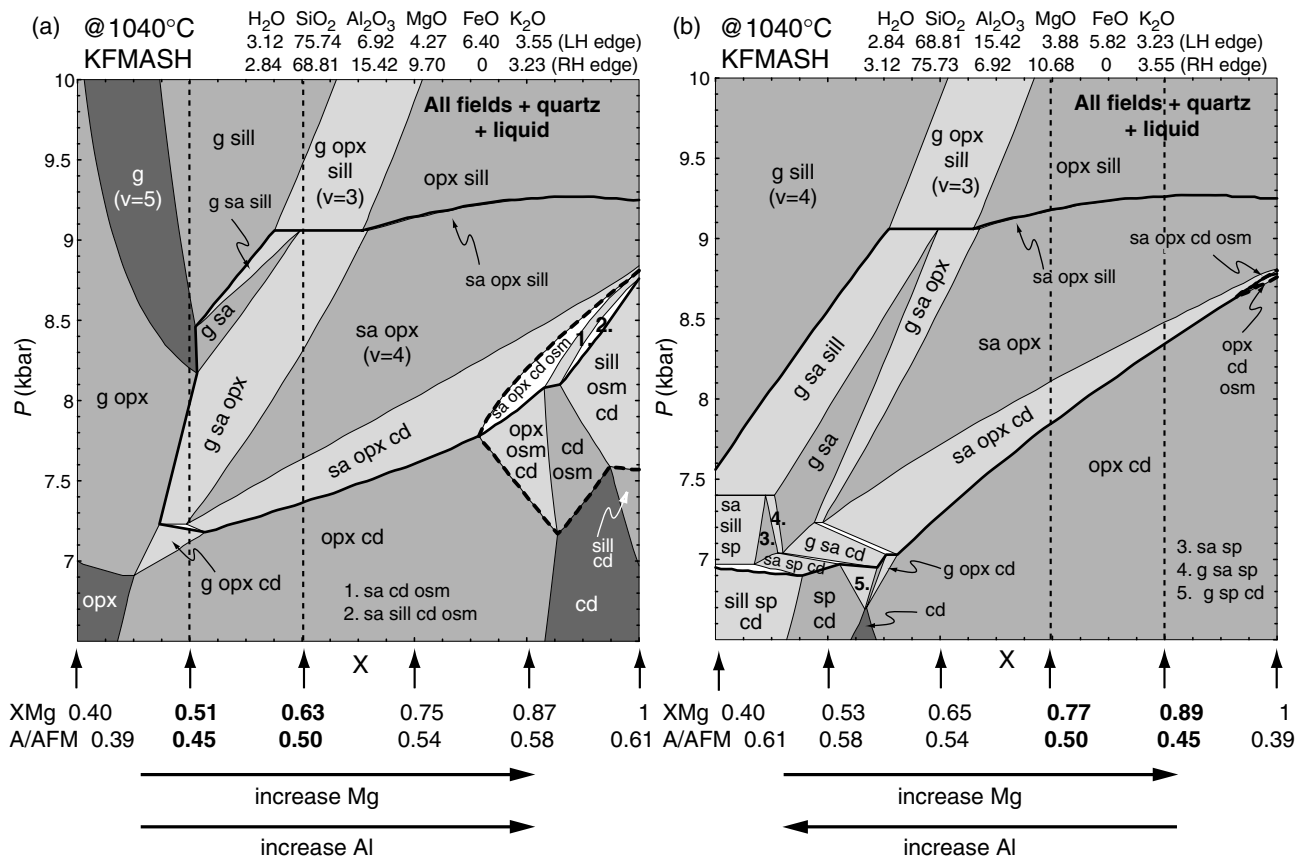


Fig. 7. *P-X* pseudosections calculated at 1040 °C for bulk compositions with varying alumina and iron-magnesium given by compositions (mol.%) above pseudosections. (a) At low alumina and X_{Mg} approximately < 0.50, sapphirine-bearing assemblages will not stabilize. Conversely sapphirine can develop at extremely high X_{Mg} . Sapphirine + quartz is destabilized at pressures above 9.5 kbar in favour of orthopyroxene-sillimanite-quartz-bearing assemblages. Garnet-sapphirine-quartz-bearing assemblages favour more iron-rich compositions, whereas osumilite stability favours high X_{Mg} . Many common granulites fall broadly in the composition realm of the left-hand side, involving garnet + orthopyroxene assemblages. (b) With a highly aluminous bulk composition (left-hand side), sapphirine can stabilize in relatively iron-rich bulk compositions (e.g. X_{Mg} < 0.50; the assemblage sa + g + sill; Sandiford, 1985). Sapphirine + sillimanite assemblages are facilitated in both 'Fe-Al-rich' (as sa + sill + g) and Mg-Al-rich (as sa + sill + opx) compositions. Although spinel stability is indicated below about 7.4 kbar, the common presence of Zn and/or Cr and/or Fe³⁺ in spinel probably makes these calculated spinel-bearing phase relations inapplicable to many natural occurrences. Note that the disposition of fields identical to both (a) and (b) is similar, highlighting the role of bulk iron-magnesium on sapphirine stability. Vertical dashed lines indicate compositions at which *P-T* pseudosections (Fig. 8) are calculated. Other bold, dashed and thick bold lines delineate sapphirine and osumilite stability and univariant reactions respectively. Variance, *v*, of fields as indicated.

variant *P-T* projection, Fig. 3. All calculated pseudosections show that mineral assemblage evolution in KFMASH is dominated by non-univariant, high-variance ($v \geq 2$), continuous, reaction processes. Consequently an individual KFMASH bulk composition, as used in experiments and pseudosection calculations, reveals potentially little about the true complexity of the underlying KFMASH univariant reaction framework (compare Figs 8 & 3). Conversely, despite the *P-T* projection (Fig. 3) indicating sapphirine-quartz stability to extend over a considerable arc of *P-T* space, many of these equilibria will not be 'seen' by a specific bulk composition. Moreover, univariant equilibria characterized by a limited range in phase compositions can only be 'seen' by a restricted range of bulk compositions. Consequently, interpreting mineral assemblage evolution in terms of discontinuous (univariant) reaction

processes alone is likely to be misleading, particularly for establishing tightly constrained *P-T* histories. The expansion to systems larger than KFMASH, and hence even more closely representative of real systems, will generally result in a variance increase for a particular mineral assemblage (e.g. White *et al.*, 2002; Kelsey *et al.*, 2003a), thereby further exacerbating the inapplicability of the use of only univariant reactions to interpret mineral assemblage evolution histories.

The wedge-shaped field of sapphirine + quartz stability (Figs 5 & 8) may impact quite strongly on the textural development of rocks that reach such extreme temperatures. Indeed, it is not until temperatures exceed about 1050 °C that sapphirine is stable over ≥ 1.5 –2 kbar pressure range for the investigated bulk compositions. This is in part a function of the strong influence of the degenerate KFMASH univariant

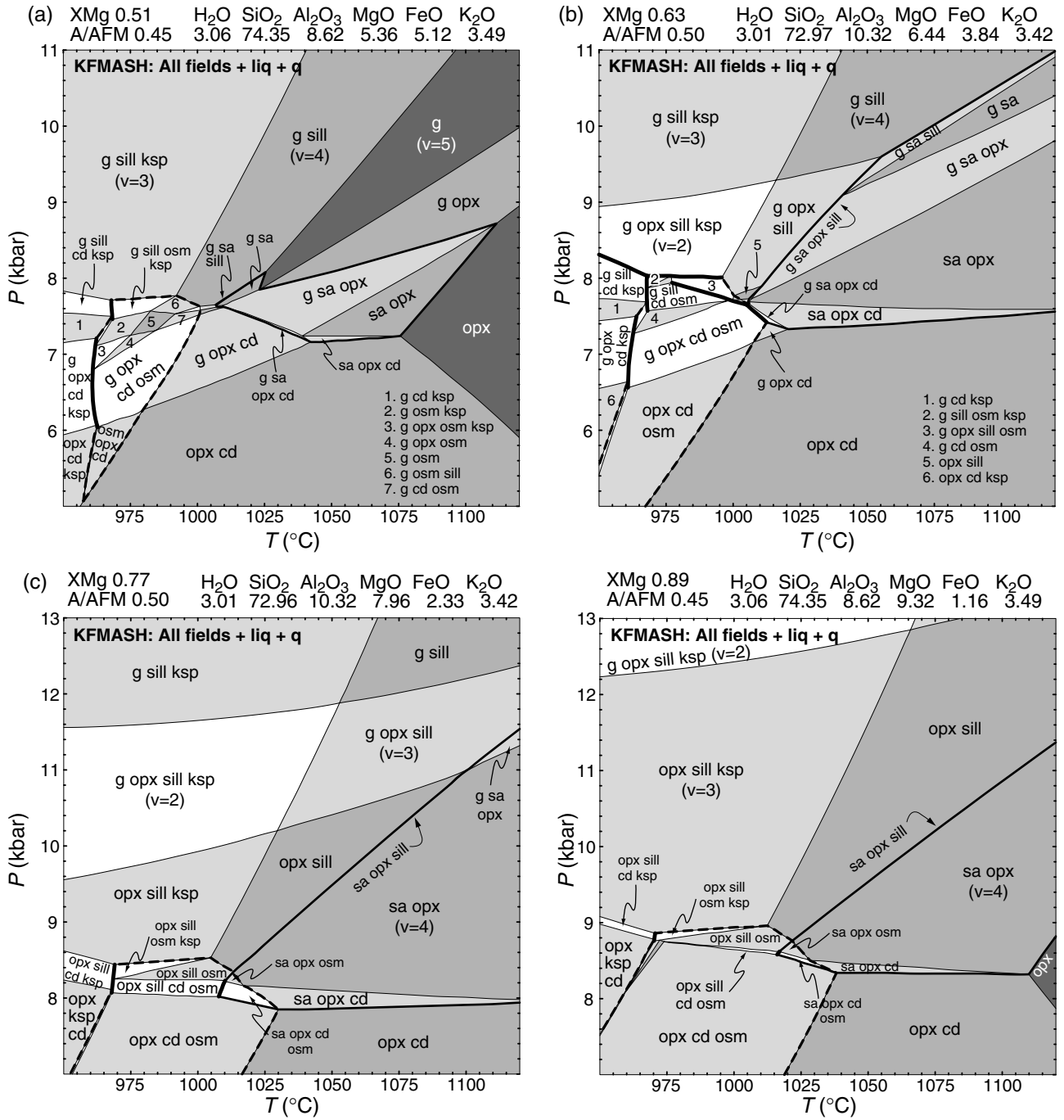


Fig. 8. *P*–*T* pseudosections calculated for compositions marked by vertical dashed lines in Figs 6 & 7. Alumina ratio is constant in (a) and (d), and also in (b) and (c). *X*_{Mg} increases from (a) to (d). The pseudosections are dominated by multi-variant ($v \geq 2$) equilibria. The *P*–*T* stability range of depicted assemblages (e.g. g + sa + q) for a given bulk composition is much restricted compared with that suggested by the *P*–*T* grid, Fig. 3. Sapphirine stability, shown by bold lines, is much restricted in more Fe-rich rocks (a). Osumilite stability, shown by dashed lines, is more restricted in a more hydrous bulk composition (compare Fig. 5; Hensen, 1977). Thick bold lines delineate univariant reactions.

reaction $\text{opx} + \text{sill} \pm \text{g} = \text{sa} + \text{q} \pm \text{g}$ on restricting sapphirine stability (Figs 5 & 8). There are in fact very few reported natural examples of sapphirine + quartz associations in Fe³⁺-poor rocks (e.g. Enderby Land, Antarctica: Ellis *et al.*, 1980; Grew, 1980; Sandiford,

1985; Motoyoshi & Hensen, 1989; Harley & Motoyoshi, 2000; Hollis & Harley, 2002; Brazil: Moraes *et al.*, 2002), most likely reflecting the extreme metamorphic conditions required for sapphirine + quartz stability. In contrast there are a greater

reported number of sapphirine + quartz occurrences in more oxidized rocks (e.g. India: Lal *et al.*, 1987; Uganda: Sandiford *et al.*, 1987; Canada: Currie & Gittins, 1988; Algeria: Bertrand *et al.*, 1992; Guiraud *et al.*, 1996), a probable consequence of sapphirine + quartz apparently being stabilized to lower temperatures by Fe^{3+} (e.g. Powell & Sandiford, 1988).

Given the tapering wedge-shape of sapphirine + quartz stability occurring at the extreme thermal end of crustal metamorphism, the development and preservation of sapphirine will be a function of many interacting factors, including: (i) the locus of the P - T path through the sapphirine + quartz stability field(s), (ii) the rate at which a rock travels through the sapphirine + quartz field(s), (iii) reaction kinetics, leading to texture development, which are controlled by the efficiency of elemental diffusion by physical and chemical processes (e.g. Spear, 1993; Stüwe, 1997; Brown, 2002). Diffusional efficiency, in turn, is controlled by factors such as the distribution and amount of silicate melt within an equilibration volume (e.g. White & Powell, 2002; analogous to Rubie, 1986; Ashworth, 1993; Yund, 1997; Guiraud *et al.*, 2001), and temperature (e.g. Stüwe, 1997). Elemental diffusion rates must exceed the rate at which a rock traverses the sapphirine + quartz field(s) if sapphirine is to develop in large proportions and/or achieve coarse grain sizes. Conversely, for sapphirine to be preserved, the efficiency of elemental diffusion must be significantly retarded as sapphirine will be the first mineral to be consumed by exiting the sapphirine + quartz field(s). That sapphirine + quartz mineral assemblages are preserved implies that kinetic processes acting during their development have since been retarded (e.g. Kelsey *et al.*, 2003a).

Coronae and/or symplectites of orthopyroxene + sillimanite or garnet + sillimanite post-dating and thus isolating sapphirine from quartz are documented from a number of localities in both Fe^{3+} -poor and Fe^{3+} -bearing rocks (e.g. Antarctica: Ellis *et al.*, 1980; Grew, 1980; Sandiford, 1985; Hollis & Harley, 2002; Canada: Morse & Talley, 1971; Currie & Gittins, 1988; India: Lal *et al.*, 1987; Kamineni & Rao, 1988; Bose *et al.*, 2000; Brazil: Moraes *et al.*, 2002). Less commonly, sapphirine + quartz are interpreted as post-dating orthopyroxene + sillimanite \pm garnet assemblages (e.g. Algeria: Bertrand *et al.*, 1992; Guiraud *et al.*, 1996; Ouzegane & Boumaza, 1996). Cordierite-bearing mineral reaction textures are also commonly documented together with sapphirine + quartz assemblages. Cordierite development is typically interpreted as post-dating orthopyroxene + sillimanite coronae and symplectites (e.g. Leong & Moore, 1972; Ellis *et al.*, 1980; Lal *et al.*, 1987; Kamineni & Rao, 1988; Baba, 1999), and more rarely as pre-dating sapphirine + quartz (e.g. Motoyoshi & Hensen, 1989).

Detailed information regarding both the P - T conditions and the P - T path locus that resulted in textural development such as that above is very difficult to

establish using the univariant grid approach. For example, whereas sapphirine + quartz with garnet is suggested to be stable over a large range of P - T on P - T grids (Fig. 3), pseudosections show that the P - T stability of garnet + sapphirine + quartz is actually relatively restricted, and its location highly sensitive to bulk composition (Fig. 8). Similarly, sapphirine + cordierite + quartz stability is considerably restricted on P - T pseudosections (Fig. 8) when compared with the P - T grid. Further, little certain information regarding the locus of the P - T path can be established using just the univariant P - T grid approach. With the aid of P - T pseudosections, which display the disposition and size/extent of assemblage fields with respect to each other, one can attempt to rigorously distinguish, for example, whether development of orthopyroxene + sillimanite or garnet + sillimanite after sapphirine + quartz is the result of cooling and/or compression (Fig. 8).

Rocks from the Napier Complex in Enderby Land, Antarctica, are the best-studied example of low- Fe^{3+} sapphirine + quartz granulites. Documented rocks from there encompass a wide array of sapphirine-quartz-bearing and other granulite facies assemblages. In the following, assemblages and/or reaction textures from the Napier Complex are explored via the use of the P - T pseudosections in Fig. 8. The pseudosections, although general, allow the P - T evolution of the Napier Complex to be investigated, and provide insight that is consistent with the previously interpreted evolution. Some inconsistencies regarding the P - T conditions of metamorphism, introduced via the use of FMAS grids, are also clarified.

Granulites from the Napier Complex are historically cited as preserving evidence of a near-isobaric-cooling P - T path (Ellis, 1980; Ellis & Green, 1985; Harley, 1985; Sandiford, 1985). A pressure gradient is believed to exist over the terrane, whereas peak temperatures are consistent across the terrane (e.g. Sandiford, 1989). Pressures of about 6–8 and >8 kbar are retrieved from the northern and southern Napier Complex respectively on the basis of thermobarometry (e.g. Grew, 1980; Sheraton *et al.*, 1980; Harley, 1985, 1998b). An anticlockwise P - T evolution is suggested on the basis of early cordierite-bearing assemblages (e.g. sapphirine + cordierite + quartz; Motoyoshi & Hensen, 1989; Hollis & Harley, 2002). Some confusion regarding the pressure(s) of metamorphism in the Napier Complex has been introduced with the use of FMAS grids, which suggest pressures of >11 kbar, the estimated position of FMAS [sp], for the development of diagnostic mineral assemblages (e.g. sapphirine + orthopyroxene + sillimanite + quartz, garnet + sapphirine + orthopyroxene + quartz and garnet + sapphirine + sillimanite + quartz; Harley, 1998b; Hollis & Harley, 2002). However, other assemblages, such as early-cordierite-bearing (e.g. Motoyoshi & Hensen, 1989; Hollis & Harley, 2002) and some quartz-absent assemblages (Harley, 1986), from the same or nearby localities, suggest pressures

lower than FMAS [sp]. This example highlights the influence of H₂O, for example, on FMAS equilibria for a specific bulk composition. Moreover, pressures suggested by FMAS grids conflict with existing barometry (e.g. Hollis & Harley, 2002).

For the purposes of the discussion, the four compositions used in Fig. 8 can be considered to represent four different rocks from Enderby Land, either from the same or different localities. Thus, the pseudosections demonstrate that the advocated cooling-dominated *P*–*T* history can result in markedly different mineral assemblage and mineral textural development in different rocks, depending upon the pressure.

Pressures above 8.5–9 kbar correspond to those estimated for the southern Napier Complex. Osumilite + quartz is rare in the southern Napier Complex. The pseudosections indicate that sapphirine is likely to be observed only within rocks that are relatively magnesian (compare Fig. 8b–d with 8a). In the most magnesian rocks, cooling products may only involve orthopyroxene + sillimanite (e.g. Fig. 8c,d; Sandiford, 1985; Harley & Hensen, 1990), whereas more Fe-rich rocks (e.g. Fig. 8b,c) may be characterized by sillimanite ± orthopyroxene ± garnet cooling textures (e.g. Sandiford, 1985). The rarity of osumilite in the southern Napier Complex (e.g. Ellis *et al.*, 1980; Sandiford, 1985) probably indicates that pressures exceeded about 9 kbar. Pressures >8 kbar are above [bi ksp sp], the KFMASH analogue of the FMAS [sp] invariant point, and hence pressures of >11 kbar, implied by some FMAS grids, are not necessary to develop the diagnostic assemblages sapphirine + orthopyroxene + sillimanite + quartz, garnet + sapphirine + orthopyroxene + quartz and garnet + sapphirine + sillimanite + quartz.

Contrasting with the southern Napier Complex, the northern Napier Complex contains a greater abundance of osumilite-quartz-bearing assemblages and osumilite breakdown textures, and lesser orthopyroxene + sillimanite + quartz assemblages (Ellis *et al.*, 1980). Assemblages calculated at pressures lower than about 9 kbar (Fig. 8) are able to account for many of the quartz-bearing assemblages of the northern Napier Complex, including osumilite replacement symplectites orthopyroxene + sillimanite + cordierite + K-feldspar + quartz (e.g. Fig. 8c,d; Hollis & Harley, 2002), osumilite replacement symplectites orthopyroxene + cordierite + K-feldspar + quartz (e.g. Fig. 8c,d; Ellis *et al.*, 1980), early cordierite-sapphirine-quartz assemblages (e.g. Fig. 8c,d; Motoyoshi & Hensen, 1989), sapphirine-orthopyroxene-quartz assemblages (e.g. Fig. 8d; Harley & Motoyoshi, 2000), garnet-sapphirine-quartz-bearing assemblages (e.g. Fig. 8b; Hollis & Harley, 2002), garnet + osumilite assemblages (Ellis *et al.*, 1980; Grew, 1980), garnet-cordierite-sapphirine-quartz assemblages (e.g. Fig. 8a,b; Harley & Hensen, 1990; Hollis & Harley, 2002) and several other assemblages documented in Ellis *et al.* (1980). Moreover, given favourable kinetics and *dT/dt*,

calculated pseudosections indicate that the bulk-compositional range of rocks in which sapphirine-quartz may occur in the northern Napier Complex is greater (i.e. includes Fig. 8a) than that of the southern Napier Complex.

The broad application of calculated pseudosections is able to predict many of the mineral assemblages and reaction textures documented from Enderby Land. The disposition of assemblage fields on the calculated pseudosections implies that the interpretation of an anticlockwise evolution involving early cordierite-bearing assemblages, followed by a near-isobaric cooling path, is supported. The pressures at which this evolution takes place lie between approximately 7 and 9–10 kbar, with no requirement for the higher pressures suggested by some FMAS grids. This result is consistent with existing barometry (e.g. Grew, 1980; Sheraton *et al.*, 1980; Harley, 1985, 1998b). The development of cordierite post-dating orthopyroxene + sillimanite (Ellis *et al.*, 1980), for example, is consistent with a small amount of decompression with cooling.

CONCLUSIONS

The sapphirine *a*-*x* model presented here is an improvement on the previous Holland & Powell (1998) model, and enables reconstruction of natural mineral assemblages and compositions in rocks containing minimal Fe³⁺. However, remaining uncertainty associated with the model stems largely from a paucity of experimental data monitoring sapphirine composition variability with changing *P*–*T* in geologically realistic chemical systems. Future improvements for the model involving the magnitude and variability of *x*_{sa} and *y*_{sa} with *P*–*T* and other phases should arise with additional experimental work on sapphirine stability. In addition, the incorporation of Fe³⁺ into the sapphirine model will allow for the detailed interpretation of assemblages in appreciably oxidized rocks.

This study demonstrates that the new *a*-*x* model for sapphirine allows calculations within KFMASH and its subsystems, presented here in the presence of quartz. Due to the effect of H₂O on the location of mineral equilibria in FMAS(H), difficulties are likely to arise in using such a grid to decipher the *P*–*T* evolution of rocks from the same terrain that may involve differing *a*_{H₂O}. Therefore as H₂O is an important rock-forming component, which along with K₂O for example, should be included when deriving grids and particularly determining the *P*–*T* evolution of mineral assemblages.

The sapphirine + osumilite-bearing portion of the KFMASH petrogenetic (*P*–*T*) grid is more complex than existing qualitative and semi-quantitative grids (e.g. FMAS). As a rock with specific bulk composition will dominantly involve high-variance (*v* ≥ 2) mineral assemblages in KFMASH, the full complexity of the high-temperature portion of the petrogenetic grid is difficult to realize on the basis of experimental results, natural assemblages and calculated *P*–*T* pseudosec-

tions. Further, use of the petrogenetic grid to interpret the evolution of mineral assemblages is limiting as the P - T stability range of a multi-variant mineral assemblage depicted on a pseudosection commonly differs, sometimes greatly, from that suggested by the P - T grid. Calculated projections and pseudosections predict mineral compositions and assemblage field topology consistent with experimental and natural data. In addition, calculated phase diagrams consistently predict natural low- Fe^{3+} sapphirine-quartz-bearing assemblages and mineral reaction sequences from Enderby Land, Antarctica. Therefore pseudosections calculated for sapphirine-bearing rocks may be able to more thoroughly shed light on the metamorphic conditions associated with ultrahigh-temperature crustal metamorphism, given detailed knowledge of the bulk composition of a mineral reaction texture(s). Finally, the KFMASH sapphirine model provides a basis for expansion to larger, even more geologically realistic chemical systems.

ACKNOWLEDGEMENTS

Research was funded by an Australian Research Council Discovery Grant to RP, RWW and G. Clarke (DP0209461). S. Harley, J. Baldwin and J. Hollis are thanked for thorough and constructive reviews. DEK was funded by an Australian Postgraduate Award during his PhD.

REFERENCES

- Ackermann, D., Seifert, F. & Schreyer, W., 1975. Instability of sapphirine at high pressures. *Contributions to Mineralogy and Petrology*, **50**, 79–92.
- Annersten, H. & Seifert, F., 1981. Stability of the assemblage orthopyroxene-sillimanite-quartz in the system $\text{MgO-FeO-Fe}_2\text{O}_3\text{-Al}_2\text{O}_3\text{-SiO}_2\text{-H}_2\text{O}$. *Contributions to Mineralogy and Petrology*, **77**, 158–165.
- Arima, M. & Gower, C. F., 1991. Osumilite-bearing granulites in the eastern Grenville Province, eastern Labrador, Canada: mineral parageneses and metamorphic conditions. *Journal of Petrology*, **32**, 29–61.
- Ashworth, J. R., 1993. Fluid-absent diffusion kinetics of Al inferred from retrograde metamorphic coronas. *American Mineralogist*, **78**, 331–337.
- Audibert, N., Bertrand, P., Hensen, B. J., Kienast, J. R. & Ouzegane, K., 1993. Cordierite-K-feldspar-quartz-orthopyroxene symplectite from southern Algeria: new evidence for osumilite in high-grade metamorphic rocks. *Mineralogical Magazine*, **57**, 354–357.
- Audibert, N., Hensen, B. J. & Bertrand, P., 1995. Experimental study of phase relations involving osumilite in the system $\text{K}_2\text{O-FeO-MgO-Al}_2\text{O}_3\text{-SiO}_2\text{-H}_2\text{O}$ at high pressure and temperature. *Journal of Metamorphic Geology*, **13**, 331–344.
- Baba, S., 1999. Sapphirine-bearing orthopyroxene-kyanite/sillimanite granulites from South Harris, NW Scotland: evidence for Proterozoic UHT conditions in the Lewisian. *Contributions to Mineralogy and Petrology*, **136**, 33–47.
- Berg, J. H. & Wheeler, E. P., 1976. Osumilite of deep-seated origin in contact aureole of the anorthositic Nain complex, Labrador. *American Mineralogist*, **61**, 29–37.
- Bertrand, P., Ellis, D. J. & Green, D. H., 1991. The stability of sapphirine-quartz and hypersthene-sillimanite-quartz assemblages: an experimental investigation in the system $\text{FeO-MgO-Al}_2\text{O}_3\text{-SiO}_2$ under H_2O and CO_2 conditions. *Contributions to Mineralogy and Petrology*, **108**, 55–71.
- Bertrand, P., Ouzegane, Kh. & Kienast, J. R., 1992. P - T - X relationships in the Precambrian Al-Mg-rich granulites from In Ouzzal, Hoggar, Algeria. *Journal of Metamorphic Geology*, **10**, 17–31.
- Bose, S., Fukuoka, M., Sengupta, P. & Dasgupta, S., 2000. Evolution of high-Mg-Al granulites from Sunkarametta, Eastern Ghats, India: evidence for a lower crustal heating-cooling trajectory. *Journal of Metamorphic Geology*, **18**, 223–240.
- Brown, M., 2002. Retrograde processes in migmatites and granulites revisited. *Journal of Metamorphic Geology*, **20**, 25–40.
- Caporuscio, F. A. & Morse, S. A., 1978. Occurrence of sapphirine plus quartz at Peekskill, New York. *American Journal of Science*, **278**, 1334–1342.
- Carrington, D. P. & Harley, S. L., 1995a. Partial melting and phase relations in high-grade metapelites: an experimental petrogenetic grid in the KFMASH system. *Contributions to Mineralogy and Petrology*, **120**, 270–291.
- Carrington, D. P. & Harley, S. L., 1995b. The stability of osumilite in metapelitic granulites. *Journal of Metamorphic Geology*, **13**, 613–625.
- Christy, A. G., Phillips, B. L., Güttler, B. K. & Kirkpatrick, R. J., 1992. A ^{27}Al and ^{29}Si MAS NMR and infrared spectroscopic study of Al-Si ordering in natural and synthetic sapphirine. *American Mineralogist*, **77**, 8–18.
- Currie, K. L. & Gittins, J., 1988. Contrasting sapphirine parageneses from Wilson Lake, Labrador and their tectonic implications. *Journal of Metamorphic Geology*, **6**, 603–622.
- Das, K., Dasgupta, S. & Miura, H., 2001. Stability of osumilite coexisting with spinel solid solution in metapelitic granulites at high oxygen fugacity. *American Mineralogist*, **86**, 1423–1434.
- Das, K., Dasgupta, S. & Miura, H., 2003. An experimentally constrained petrogenetic grid in the silica-saturated portion of the system KFMASH at high temperatures and pressures. *Journal of Petrology*, **44**, 1055–1075.
- Dasgupta, S., Sengupta, P., Ehl, J., Raith, M. & Bardhan, S., 1995. Reaction textures in a suite of spinel granulites from the Eastern Ghats Belt, India: evidence for polymetamorphism, a partial petrogenetic grid in the system KFMASH and the roles of ZnO and Fe_2O_3 . *Journal of Petrology*, **36**, 435–461.
- Doroshev, A. M. & Malinovsky, I. Y., 1974. Upper pressure limit of stability of sapphirine. *Doklady Akademiia Nauk SSSR*, **219**, 136–138.
- Ellis, D. J., 1980. Osumilite-sapphirine-quartz granulites from Enderby Land, Antarctica: P - T conditions of metamorphism, implications for garnet-cordierite equilibria and the evolution of the deep crust. *Contributions to Mineralogy and Petrology*, **74**, 201–210.
- Ellis, D. J. & Green, D. H., 1985. Garnet-forming reactions in mafic granulites from Enderby Land, Antarctica – mineral assemblages and reactions. *Journal of Petrology*, **26**, 633–662.
- Ellis, D. J., Sheraton, J. W., England, R. N. & Dallwitz, W. B., 1980. Osumilite-sapphirine-quartz granulites from Enderby Land, Antarctica: mineral assemblages and reactions. *Contributions to Mineralogy and Petrology*, **72**, 123–143.
- Grew, E. S., 1980. Sapphirine + quartz association from Archaean rocks in Enderby Land, Antarctica. *American Mineralogist*, **65**, 821–836.
- Grew, E. S., 1982. Osumilite in the sapphirine-quartz terrane of Enderby Land, Antarctica: implications for osumilite petrogenesis in the granulite facies. *American Mineralogist*, **67**, 762–787.
- Guiraud, M., Kienast, J. R. & Rahmani, A., 1996. Petrological study of high-temperature granulites from In Ouzzal, Algeria: some implications on the phase relationships in the FMAS-TOCr system. *European Journal of Mineralogy*, **8**, 1375–1390.
- Guiraud, M., Powell, R. & Rebay, G., 2001. H_2O in metamorphism and unexpected behaviour in the preservation of metamorphic mineral assemblages. *Journal of Metamorphic Geology*, **19**, 445–454.

- Harley, S. L., 1985. Garnet-orthopyroxene bearing granulites from Enderby Land, Antarctica. Metamorphic pressure-temperature-time evolution of the Archaean Napier Complex. *Journal of Petrology*, **26**, 819–856.
- Harley, S. L., 1986. A sapphirine-cordierite-garnet-sillimanite granulite from Enderby Land, Antarctica: implications for FMAS petrogenetic grids in the granulite facies. *Contributions to Mineralogy and Petrology*, **94**, 452–460.
- Harley, S. L., 1989. The origins of granulites: a metamorphic perspective. *Geological Magazine*, **126**, 215–247.
- Harley, S. L., 1998a. On the occurrence and characterisation of ultrahigh-temperature (UHT) crustal metamorphism. In: *What Drives Metamorphic Reactions? Special Publication 138* (eds Treloar, P. J. & O'Brien, P.), pp. 75–101. Geological Society, London.
- Harley, S. L., 1998b. An appraisal of peak temperatures and thermal histories in ultrahigh-temperature (UHT) crustal metamorphism: the significance of aluminous orthopyroxene. *Memoirs of the National Institute of Polar Research, Special issue*, **53**, 49–73.
- Harley, S. L. & Hensen, B. J., 1990. Archaean and Proterozoic high-grade terranes of East Antarctica (40–80 °E): a case study of diversity in granulite facies metamorphism. In: *High-temperature metamorphism and Crustal Anatexis, Series 2* (eds Ashworth, J.R. & Brown, M.), pp. 320–370, The Mineralogical Society of Great Britain, Unwin-Hyman.
- Harley, S. L. & Motoyoshi, Y., 2000. Al zoning in orthopyroxene in a sapphirine quartzite: evidence for > 1120 °C UHT metamorphism in the Napier Complex, Antarctica, and implications for the entropy of sapphirine. *Contributions to Mineralogy and Petrology*, **138**, 293–307.
- Hensen, B. J., 1971. Theoretical phase relations involving cordierite and garnet in the system MgO-FeO-Al₂O₃-SiO₂. *Contributions to Mineralogy and Petrology*, **33**, 191–214.
- Hensen, B. J., 1972. Phase relations involving pyrope, enstatite_{ss} and sapphirine_{ss} in the system MgO-Al₂O₃-SiO₂. *Carnegie Institute of Washington Yearbook*, **71**, 421–427.
- Hensen, B. J., 1977. The stability of osumilite in high grade metamorphic rocks. *Contributions to Mineralogy and Petrology*, **64**, 197–204.
- Hensen, B. J., 1986. Theoretical phase relations involving cordierite and garnet revisited: the influence of oxygen fugacity on the stability of sapphirine and spinel in the system Mg-Fe-Al-Si-O. *Contributions to Mineralogy and Petrology*, **92**, 362–367.
- Hensen, B. J. & Green, D. H., 1971. Experimental study of the stability of cordierite and garnet in pelitic compositions at high pressures and temperatures. *Contributions to Mineralogy and Petrology*, **33**, 309–330.
- Hensen, B. J. & Green, D. H., 1973. Experimental study of the stability of cordierite and garnet in pelitic compositions at high pressures and temperatures. III. Synthesis of experimental data and geological applications. *Contributions to Mineralogy and Petrology*, **38**, 151–166.
- Hensen, B. J. & Harley, S. L., 1990. Graphical analysis of *P-T-X* relations in granulite facies metapelites. In: *High-Temperature Metamorphism and Crustal Anatexis, Series 2* (eds Ashworth, J.R. & Brown, M.), pp. 19–56, The Mineralogical Society of Great Britain, Unwin-Hyman.
- Higgins, J. B., Ribbe, P. H. & Herd, R. K., 1979. Sapphirine I: crystal chemical contributions. *Contributions to Mineralogy and Petrology*, **68**, 349–356.
- Holland, T. J. B. & Powell, R., 1998. An internally consistent thermodynamic data set for phases of petrological interest. *Journal of Metamorphic Geology*, **16**, 309–343.
- Holland, T. J. B., Babu, E. V. S. S. K. & Waters, D. J., 1996. Phase relations of osumilite and dehydration melting in pelitic rocks: a simple thermodynamic model for the KFMASH system. *Contributions to Mineralogy and Petrology*, **124**, 383–394.
- Hollis, J. A. & Harley, S. L., 2002. New evidence for the peak temperatures and the near-peak pressure-temperature evolution of the Napier Complex. *Royal Society of New Zealand Bulletin*, **35**, 19–29.
- Hollis, J. A. & Harley, S. L., 2003. Alumina solubility in orthopyroxene coexisting with sapphirine and quartz. *Contributions to Mineralogy and Petrology*, **144**, 473–483.
- Kaminen, D. C. & Rao, A. T., 1988. Sapphirine-bearing quartzite from the Eastern Ghats terrain, Vizianagaram, India. *Journal of Geology*, **96**, 209–220.
- Kelsey, D., White, R. W. & Powell, R., 2003a. Orthopyroxene-sillimanite-quartz assemblages: distribution, petrology, quantitative *P-T-X* constraints and *P-T* paths. *Journal of Metamorphic Geology*, **21**, 439–453.
- Kelsey, D., White, R. W., Powell, R., Wilson, C. J. L. & Quinn, C. D., 2003b. New constraints on metamorphism in the Rauer Group, Prydz Bay, east Antarctica. *Journal of Metamorphic Geology*, **21**, 739–759.
- Lal, R. K., Ackermann, D. & Upadhyay, H., 1987. *P-T-X* relationships deduced from corona textures in sapphirine-spinel-quartz assemblages from Paderu, southern India. *Journal of Petrology*, **28**, 1139–1169.
- Leong, K. M. & Moore, J. M., 1972. Sapphirine-bearing rocks from Wilson Lake, Labrador. *Canadian Mineralogist*, **11**, 777–790.
- McDade, P. & Harley, S. L., 2001. A petrogenetic grid for aluminous granulite facies metapelites in the KFMASH system. *Journal of Metamorphic Geology*, **19**, 45–59.
- Moore, P. B., 1969. The crystal structure of sapphirine. *American Mineralogist*, **54**, 31–49.
- Moraes, R., Brown, M., Fuck, R. A., Camargo, M. A. & Lima, T. M., 2002. Characterisation and *P-T* evolution of melt-bearing ultrahigh-temperature granulites: an example from the Anápolis-Itaúcu complex of the Brasília Fold Belt, Brazil. *Journal of Petrology*, **43**, 1673–1705.
- Morse, S. A. & Talley, J. H., 1971. Sapphirine reactions in deep-seated granulites near Wilson Lake, Central Labrador, Canada. *Earth and Planetary Science Letters*, **10**, 325–328.
- Motoyoshi, Y. & Hensen, B. J., 1989. Sapphirine-quartz-orthopyroxene symplectites after cordierite in the Archaean Napier Complex, Antarctica: evidence for a counterclockwise *P-T* path? *European Journal of Mineralogy*, **1**, 467–471.
- Mouri, H., Guiraud, M. & Hensen, B., 1996. Petrology of phlogopite-sapphirine-bearing Al-Mg granulites from Ihouhouene, In Ouzal, Hoggar, Algeria: an example of phlogopite stability at high temperature. *Journal of Metamorphic Geology*, **14**, 725–738.
- Newton, R. C., 1972. An experimental determination of the high-pressure stability limits of magnesium cordierite under wet and dry conditions. *Journal of Geology*, **80**, 398–420.
- Newton, R. C., Charlu, T. V. & Kleppa, O. J., 1974. A calorimetric investigation of the stability of anhydrous magnesium cordierite with application to granulite facies metamorphism. *Contributions to Mineralogy and Petrology*, **44**, 295–311.
- Ouzegane, K. & Boumaza, S., 1996. An example of ultrahigh-temperature metamorphism: orthopyroxene-sillimanite-garnet, sapphirine-quartz and spinel-quartz parageneses in Al-Mg granulites from In Hihaou, In Ouzal, Hoggar. *Journal of Metamorphic Geology*, **14**, 693–708.
- Ouzegane, K., Guiraud, M. & Kienast, J. R., 2003. Prograde and retrograde evolution in high temperature corundum-granulites (FMAS and KFMASH systems) from In Ouzal terrane (NW Hoggar, Algeria). *Journal of Petrology*, **44**, 517–545.
- Perchuk, L. L., Aranovich, L. Ya., Podlesskii, K. K. *et al.*, 1985. Precambrian granulites of the Aldan Shield, eastern Siberia, USSR. *Journal of Metamorphic Geology*, **3**, 265–310.
- Powell, R. & Holland, T. J. B., 1988. An internally consistent thermodynamic dataset with uncertainties and correlations: 3. Application methods, worked examples and a computer program. *Journal of Metamorphic Geology*, **6**, 173–204.
- Powell, R. & Holland, T. J. B., 1999. Relating formulations of the thermodynamics of mineral solid solutions: activity modeling

- of pyroxenes, amphiboles and micas. *American Mineralogist*, **84**, 1–14.
- Powell, R. & Sandiford, M., 1988. Sapphirine and spinel phase relationships in the system FeO-MgO-Al₂O₃-SiO₂-TiO₂-O₂. *Contributions to Mineralogy and Petrology*, **98**, 64–71.
- Powell, R. & Holland, T. J. B. & Worley, B., 1998. Calculating phase diagrams involving solid solutions via non-linear equations, with examples using THERMOCALC. *Journal of Metamorphic Geology*, **6**, 173–204.
- Rubie, D. C., 1986. The catalysis of mineral reactions by water and restrictions on the presence of aqueous fluid during metamorphism. *Mineralogical Magazine*, **50**, 399–415.
- Sandiford, M., 1985. The metamorphic evolution of granulites at Fyfe Hills; implications for Archaean crustal thickness in Enderby Land, Antarctica. *Journal of Metamorphic Geology*, **3**, 155–178.
- Sandiford, M., 1989. Horizontal structures in granulite terrains: a record of mountain building or mountain collapse? *Geology*, **17**, 449–452.
- Sandiford, M., Neall, F. B. & Powell, R., 1987. Metamorphic evolution of aluminous granulites from Labwor Hills, Uganda. *Contributions to Mineralogy and Petrology*, **95**, 217–225.
- Seifert, F., 1974. Stability of sapphirine: a study of the aluminous part of the system MgO-Al₂O₃-SiO₂-H₂O. *Journal of Geology*, **82**, 173–204.
- Sengupta, P., Dasgupta, S., Battacharya, P. K., Fukuoka, M., Chakraborti, S. & Bhowmick, S., 1990. Petro-tectonic imprints in the sapphirine granulites from Anantagiri, Eastern Ghats Mobile Belt, India. *Journal of Petrology*, **31**, 971–996.
- Sheraton, J. W., Offe, L. A., Tingey, R. J. & Ellis, D., 1980. Enderby Land, Antarctica; an unusual precambrian high-grade metamorphic terrain. *Journal of the Geological Society of Australia*, **27**, 1–18.
- Spear, F., 1993. *Metamorphic Phase Equilibria and Pressure-Temperature-Time Paths*. Mineralogical Society of America, Monograph, Washington, DC.
- Steffen, G., Seifert, F. & Amthauer, G., 1984. Ferric iron in sapphirine: a Mössbauer spectroscopic study. *American Mineralogist*, **69**, 339–348.
- Stüwe, K., 1997. Effective bulk composition changes due to cooling: a model predicting complexities in retrograde reaction textures. *Contributions to Mineralogy and Petrology*, **129**, 43–52.
- Stüwe, K. & Powell, R., 1995. *P-T* paths from modal proportions: application to the Koralm Complex, Eastern Alps. *Contributions to Mineralogy and Petrology*, **119**, 83–93.
- Waters, D. J., 1986. Metamorphic history of sapphirine-bearing and related magnesian gneisses from Namaqualand, South Africa. *Journal of Petrology*, **27**, 541–565.
- White, R. W. & Powell, R., 2002. Melt loss and the preservation of granulite facies mineral assemblages. *Journal of Metamorphic Geology*, **20**, 621–632.
- White, R. W., Powell, R. & Holland, T. J. B., 2001. Calculation of partial melting equilibria in the system Na₂O-CaO-K₂O-FeO-MgO-Al₂O₃-SiO₂-H₂O (NCKFMASH). *Journal of Metamorphic Geology*, **19**, 139–153.
- White, R. W., Powell, R. & Clarke, G. L., 2002. The interpretation of reaction textures in Fe-rich metapelitic granulites of the Musgrave Block, central Australia: constraints from mineral equilibria calculations in the system K₂O-FeO-MgO-Al₂O₃-SiO₂-H₂O-TiO₂-Fe₂O₃. *Journal of Metamorphic Geology*, **20**, 41–55.
- Yund, R. A., 1997. Rates of grain boundary migration diffusion through enstatite and forsterite reaction rims. *Contributions to Mineralogy and Petrology*, **126**, 224–236.

Received 11 September 2003; revision accepted 20 May 2004.

APPENDIX A

Sapphirine

From the site mixing information provided in the text, the THERMOCALC datafile script for the new sapphirine *a-x* model is:

```

sa 3      x(sa) 0.1586
          y(sa) 0.2588

p(spr5)   1 1   0 1 1 y
p(spr4)   2 1   1 1 -1 y
          2   0 1 -1 x       1 1 -1/4 y
p(fspr)   1 2   0 1 1 x       1 1 -1/4 y

sf
W(spr5,spr4) 10 0 0
W(spr5,fspr) 12 0 0
W(spr4,fspr)  8 0 0

7      X(Fe,M1) 1 2   0 1 1 x       1 1 -1 y
        X(Mg,M1) 1 2   1 1 -1 x       1 1 -1 y
        X(Al,M1) 1 1   0 1 1 y
        X(Fe,M2) 1 1   0 1 1 x
        X(Mg,M2) 1 1   1 1 -1 x
        X(Al,T1) 1 1   0 1 1 y
        X(Si,T1) 1 1   1 1 -1 y

spr5   1 3   X(Al,M1) 1   X(Mg,M2) 3   X(Al,T1) 1
spr4   1 3   X(Mg,M1) 1   X(Mg,M2) 3   X(Si,T1) 1
fspr   1 3   X(Fe,M1) 1   X(Fe,M2) 3   X(Si,T1) 1
DQF 2 0 0

```

Osumilite

The *a-x* model for osumilite is that of Holland *et al.* (1996), involving Fe-Mg and Tschermaks substitution. For ternary (Fe-Mg-Al) osumilite two composition variables are required. Mixing occurs across multiple sites M1, T1, T2, each site respectively of multiplicity 2, 3, 2. One of these composition variables (*y*) must account for Tschermaks substitution. Let

$$x_{\text{osm}} = x_{\text{osm}}^{\text{bulk}} = \frac{2x_{\text{Fe}}^{\text{M1}} + 3x_{\text{Fe}}^{\text{T1}}}{2x_{\text{Fe}}^{\text{M1}} + 3x_{\text{Fe}}^{\text{T1}} + 2x_{\text{Mg}}^{\text{M1}} + 3x_{\text{Mg}}^{\text{T1}}}$$

$$y_{\text{osm}} = 2x_{\text{Si}}^{\text{T2}} = \text{Si}^{\text{tetrahedral,T2}} \text{ cations,}$$

where the multipliers of site fractions represent the number of cations/atoms of Fe, Mg and Si in the formula unit of end-member *i*. From these variables, the following site fractions are derived:

$$x_{\text{Fe}}^{\text{M1}} = x_{\text{osm}}$$

$$x_{\text{Mg}}^{\text{M1}} = 1 - x_{\text{osm}}$$

$$x_{\text{Al}}^{\text{M1}} = 1 - \frac{1}{3}y_{\text{osm}}$$

$$x_{\text{Fe}}^{\text{T1}} = \frac{1}{3}x_{\text{osm}}y_{\text{osm}}$$

$$x_{\text{Mg}}^{\text{T1}} = \frac{1}{3}(1 - x_{\text{osm}})y_{\text{osm}}$$

$$x_{\text{Al}}^{\text{T2}} = 1 - \frac{1}{2}y_{\text{osm}}$$

$$x_{\text{Si}}^{\text{T2}} = \frac{1}{2}y_{\text{osm}}$$

Calculation of the end-member proportions is based on $p_{\text{osm1}} + p_{\text{fosm}} + p_{\text{osm2}} = 1$. First, x_{osm} and y_{osm} are recast in terms of p 's. For example, $x_{\text{Mg}}^{\text{M1}}$ is replaced with p_{osm1} and p_{osm2} as both end-members have Mg on the M1 site. Hence,

$$x_{\text{osm}} = \frac{2p_{\text{fosm}}}{2p_{\text{fosm}} + 2p_{\text{osm1}} + 3p_{\text{osm2}}} = \frac{2p_{\text{fosm}}}{2 + 2p_{\text{osm2}}},$$

$$y_{\text{osm}} = \text{Si}^{\text{tetrahedral,T2 cations}} = p_{\text{osm2}}.$$

Substituting $y_{\text{osm}} = p_{\text{osm2}}$ into x_{osm} gives

$$x_{\text{osm}}(2 + y_{\text{osm}}) = 2p_{\text{fosm}} \rightarrow p_{\text{fosm}} = \frac{1}{2}x_{\text{osm}}(2 + y_{\text{osm}})$$

Then

$$p_{\text{osm1}} = 1 - \frac{1}{2}x_{\text{osm}}(2 + y_{\text{osm}}) - y_{\text{osm}}$$

by difference. With multiplicities of sites as given above, the ideal activity expressions are:

$$a_{\text{ideal,osm1}} = x_{\text{KMg}_2\text{Al}_3\text{Si}_{10}\text{O}_{30},\text{osumilite}} \\ = \left(x_{\text{Mg}}^{\text{M1}}\right)^2 \left(x_{\text{Al}}^{\text{T1}}\right)^3 \left(x_{\text{Al}}^{\text{T2}}\right)^2$$

$$a_{\text{ideal,fosm}} = x_{\text{KFe}_2\text{Al}_3\text{Si}_{10}\text{O}_{30},\text{osumilite}} = \left(x_{\text{Fe}}^{\text{M1}}\right)^2 \left(x_{\text{Al}}^{\text{T1}}\right)^3 \left(x_{\text{Al}}^{\text{T2}}\right)^2$$

$$a_{\text{ideal,osm2}} = x_{\text{KMg}_3\text{Al}_3\text{Si}_{11}\text{O}_{30},\text{osumilite}} \\ = 27 \left(x_{\text{Mg}}^{\text{M1}}\right)^2 \left(x_{\text{Mg}}^{\text{T1}}\right)^1 \left(x_{\text{Al}}^{\text{T1}}\right)^2 \left(x_{\text{Al}}^{\text{T2}}\right)^1 \left(x_{\text{Si}}^{\text{T2}}\right)^1$$

Note the normalization factor of 27 needed for 'osm2' in order to make its ideal activity unity. This also appears in the THERMOCALC datafile script below.

```
osm3 x(osm) 0.1722
      y(osm) 0.1774

p(osm1)  2 1  1 1 -1 y
          2 0 1 -1/2 x  2 1 1 y
p(fosm)  1 2  0 1 1/2 x  2 1 1 y
p(osm2)  1 1  0 1 1 y

sf
W(osm1,fosm)  0 0 0
W(osm1,osm2)  0 0 0
W(fosm,osm2)  0 0 0

7 X(Fe,M1)  1 1  0 1 1 x

X(Mg,M1)  1 1  1 1 -1 x
X(Al,T1)  1 1  1 1 -1/3 y
X(Mg,T1)  1 2  1 1 -1 x  0 1 1/3 y
X(Fe,T1)  1 2  0 1 1/3 x  0 1 1 y
X(Al,T2)  1 1  1 1 -1/2 y
X(Si,T2)  1 1  0 1 1/2 y

osm1 1 3 X(Mg,M) 2 X(Al,T1) 3 X(Al,T2) 2
      check 0 0 % osm1: x = 0, y = 0

fosm 1 3 X(Fe,M) 2 X(Al,T1) 3 X(Al,T2) 2
      check 1 0 % fosm: x = 1, y = 0

osm2 27 5 X(Mg,M) 2 X(Mg,T1) 1 X(Al,T1) 2 X(Al,T2) 1 X(Si,T2) 1
      check 0 1 % osm2: x = 0, y = 1
```

Remaining phases

Activity-composition models and datafile scripts, including interaction energies W_{ij} , for the solid-solution phases biotite, muscovite, garnet, orthopyroxene, cordierite, spinel and silicate melt are identical to the KFMASH models used in White *et al.* (2001).